NOVEL CATALYST SCREENING

FOR LOW TEMPERATURE NO_X ABATEMENT

by

Derek D. Falcone

A thesis submitted to the Faculty of the University of Delaware in partial fulfillment of the requirements for the degree of Bachelors in Chemical Engineering with Distinction.

Spring 2010

NOVEL CATALYST SCREENING

FOR LOW TEMPERATURE NO_X ABATEMENT

by

Derek D. Falcone

Approved: _____

Jochen Lauterbach, Ph.D.

Professor in charge of thesis on behalf of the Advisory Committee

Approved: _____

Douglas Buttrey, Ph.D

Committee member from the Department of Chemical Engineering

Approved: _____

Susan Groh, Ph.D.

Committee member from the Board of Senior Thesis Readers

Approved: _____

Ismat Shah, Ph.D.

Chair of the University Committee on Student and Faculty Honors

TABLE OF CONTENTS

LIST OF TABLES

LIST OF FIGURES

ABSTRACT

NO_x compounds are pollutants formed in fossil fuel combustion which lead to global warming, acid rain, toxic particulates and other health concerns. Due to the high activation energy of the direct decomposition reaction $2NO_x \rightarrow N_2 + xO_2$ a catalyst is needed to reduce NO_x pollution in fossil fuel burning applications which provide 85% of the worlds increasing energy demand. One of the ways to catalytically remove NO_x is through Selective Catalytic Reduction (SCR) which requires a reductant, such as ammonia, to be introduced to the effluent stream of the fossil fuel combustion. Due to the requirement of additional feed stock SCR has been heavily used in high temperature stationary applications but the desire and technology for the utilization of SCR in lower temperature automotive applications is currently emerging in the market. Therefore, a catalyst needs to be optimized that can penetrate the market to replace less fuel efficient three way catalysts (TWC).

Using a high-throughput experimentation set-up with a Fourier transform infrared (FTIR) spectrometer this work has compared 1% platinum and ruthenium catalysts synthesized via reverse micelle synthesis, which creates a narrow nanoparticle size distribution, to compare SCR activity and selectivity for the two metals. The Pt catalysts were able to maintain the conversion of NO close to or at 100% over a longer, lower (from 150 to 250^{o}C) temperature span than the Ru catalysts. The Ru catalysts were not able to reach 100% conversion until temperatures around 300^{o}C, but they were able to able to achieve a higher selectivity towards N_2 than the Pt catalysts over the entire temperature span studied. The utilization of two different surfactant chemistries was also explored. Catalysts

synthesized with a Brij-30 were able to sustain 100% or close to 100% NO conversion over a longer temperature range then catalysts synthesized with a Triton-X 100 chemistry.

A designed set of incipient wetness catalysts were screened for SCR in an attempt to find a relationship between the weight loadings of Ru and Co and the selectivity and activity in the chemistry. It was found that the 4Ru5Co15Ba, the 4Ru15Ba, and the 2.5Ru2.5Co15Ba preformed the best, in terms of activity and selectivity at 150 and 300 ^{o}C. But the relationship between the metal weight loadings and the SCR activity and selectivity was weak and unsubstantial. It was observed that a 5Co15Ba catalyst out performed other Ru catalysts with comparable activities in terms of selectivity and was deemed the cheapest most viable option out of the catalysts screened.

Chapter 1

Introduction

1.1 Selective Catalytic Reduction

1.1.1 Motivation

Approximately 85% of the world's increasing energy demand is met with the combustion of fossil fuels [1]. Among the several problems associated with combusting fossil fuels is the creation of nitric oxide (NO) and nitrous oxide (NO_2), collectively called nitrogen oxides (NO_x). Nitrogen oxides are large contributors to photochemical smog formation, acid precipitation, global warming, ozone generation in the low troposphere, and ozone layer depletion in the stratosphere [2]. Some biological studies have shown NO to be an integral component in cellular processes as an information carrier especially in the blood stream. However, when externally produced NO is introduced to the lungs the compound can diffuse through the alveolar-cells and capillary vessels provoking both infection and territory allergies like bronchitis, pneumonia, etc [3].

The two most widely used catalytic procedures currently employed to abate NO_x pollution are NO_x storage and reduction (NSR) and Selective Catalytic Reduction (SCR). NSR catalysts are most commonly used in automotive applications where the internal combustion engine cycles between a lean phase or oxygen rich phase where the nitrogen oxides are oxidized and stored on the catalytic surface, and a fuel rich phase, where the

unburned hydrocarbons and carbon monoxide released from the combustion chamber reduce the stored nitrogen oxide compounds to elemental nitrogen [4]. SCR catalysts are more commonly used in stationary applications because an additional feed of a reductant such as ammonia or urea is required [2]. However, the use of SCR catalysts for use in automotive applications will be increasingly desired because of increased federal NO_x emissions regulations implemented by the Obama administration [5]. In January of 2010 the EPA also strengthened the health-based National Ambient Air Quality Standard (NAAQS) for nitrogen dioxide [6]. The new standard will call for the reduction of NO_2 pollution across all NO_x polluting sectors. Figure 1 shows the percentage of NO_x pollution by sector; in both the United States and Europe in the transportation sector contributes to approximately half of the NO_x pollutants in the atmosphere.

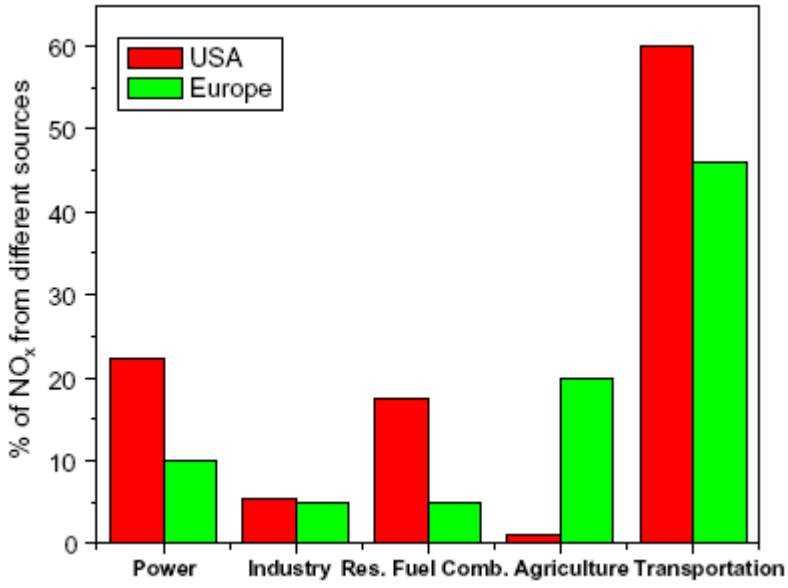

Figure 1 Production of NO_x by sector in the USA and Europe (reproduced from [3])

1.1.2 Mechanism

The average NO_x emission from gasoline, which combusts at 870°C, engine exhaust is typically 95% NO and 5% NO_2 and is created through one of three mechanisms. The mechanism that typically contributes to automotive exhaust the most is *thermal* NO_x which comes from the oxidation of elemental nitrogen in the air at high temperatures which is described in Equation 1.

$$N_2 + O_2 \leftrightarrow 2NO \qquad \Delta H^\circ = 180.6 \ \frac{kJ}{mol} \tag{1}$$

This reaction, whose rate increases exponentially with temperature, is controlled by the Zeldovich mechanism and occurs above 1300 K [3]. The proliferation of this reaction can be controlled by lowering the temperature of combustion or by running the engine under lean conditions but these measures have been shown to be ineffective because they lower the efficiency of the engine [7].

The second mechanism of NO_x formation is called *fuel* NO_x and comes from the oxidation of nitrogen present in the fossil fuel. The production of *fuel* NO_x from the combustion of biomass also occurs by a similar mechanism but the process to reduce NO_x from biofuels is different and will not be discussed in the work[8]. Unlike *thermal* NO_x the creation of *fuel* NO_x is not a strong function of combustion temperature within the range of normal internal combustion engine temperatures [3].

The third mechanism of NO_x formation is called *prompt* NO_x also called Fenimore NO. The creation of NO_x by this route occurs through the reaction of unburned hydrocarbons with atmospheric nitrogen downstream from the combustion engine; these species are then oxidized to NO in the lean zone of the flame. The formation of *prompt* NO_x is

proportional to the number of carbon atoms present per unit volume of the parent hydrocarbon and can be formed in a significant quantity at low-temperatures and fuel-rich conditions and where residence times are short [3]. NO can also further react with oxygen to form NO_2 and N_2O by the following two reactions:

$$N_2 + \frac{1}{2}O_2 \leftrightarrow NO_2 \qquad \Delta H^\circ = -113\ \frac{kJ}{mol} \tag{2}$$

$$2NO \leftrightarrow N_2O + \frac{1}{2}O_2 \qquad \Delta H^\circ = -99\ \frac{kJ}{mol} \tag{3}$$

NO has a positive standard free energy of formation at ambient and relatively high temperatures [9] therefore the following decomposition reaction

$$NO \leftrightarrow \frac{1}{2}N_2 + \frac{1}{2}O_2 \tag{4}$$

is thermodynamically favorable. However, homogenous decomposition is immeasurably slow in the absence of a catalyst because the rightward reaction of reaction 4 has a very high activation energy (364 kJ/mol) [3]. Forcing reaction 4 to the right also becomes increasingly more difficult in an environment exposed to air. By LeChatelier's principle high partial pressures of N_2 and O_2 will shift the equilibrium of reaction 4 to the left. Furthermore in an oxygen rich environment at moderate temperatures the oxidation of NO to NO_2 following reaction 5 becomes significant.

$$NO + \frac{1}{2}O_2 \leftrightarrow NO_2 \tag{5}$$

Therefore, an effective NO_x decomposition catalyst—i.e. one that drives reactions 4 and 5 completely to equilibrium—that can reduce the concentration of NO_x to levels that satisfy upcoming regulatory standards needs to be investigated [3].

Introducing an additional reductant in the exhaust of combustion process can circumvent the thermodynamic and kinetic difficulties in reducing NO_x that are inherently present in the above reactions. By selectively promoting the reaction of NO_x with a reductant over the reaction of NO_x with O_2, SCR catalysts can achieve NO_x concentrations that are below the thermodynamic equilibrium concentration [9]. However, the reaction mechanism of selectively reducing NO is complicated and still not well understood because of the many side reactions occurring between different proportions of NO, NH_3, and O_2 across different temperatures [2]. A summary of some of these side reactions is shown in Table 1 preceded by a set of reactions observed by Wang et. al. over a Cu-V/ γ-Al_2O_3 catalysts [2].

$$6NO + 4NH_3 \rightarrow 5N_2 + 6H_2O \quad (6)$$

$$4NO + 4NH_3 + O_2 \rightarrow 4N_2 + 6H_2O \quad (7)$$

$$2NO_2 + 4NH_3 + O_2 \rightarrow 4N_2 + 6H_2O \quad (8)$$

$$4NO + 4NH_3 + 3O_2 \rightarrow 4N_2O + 6H_2O \quad (9)$$

$$2NH_3 + \frac{5}{2}O_2 \rightarrow 2NO + 6H_2O \quad (10)$$

$$2NH_3 + 2O_2 \rightarrow N_2O + 6H_2O \quad (11)$$

$$2NO + O_2 \rightarrow 2NO_2 \quad (12)$$

$$2N_2O + 3O_2 \rightarrow 4NO_2 \quad (13)$$

$$2NH_3 + \frac{3}{2}O_2 \rightarrow N_2 + 3H_2O \quad (14)$$

Reactions 6-8 are the desired reactions out of this set. Selectivity towards the nitrogen is the ultimate goal of all SCR catalysts. The evolution of water is not ideal because it is still a green house gas but it is unavoidable when ammonia is used as the reductant since the hydrogen atoms need to be displaced somewhere in the reduction reaction. As can be seen from above the other undesirable products that arise from the reduction of NO with NH_3 in the presence of O_2 and N_2 are NO_2 and N_2O.

N_2O is a powerful green house gas and has been shown to cause the depletion of stratospheric ozone. Furthermore, the concentration of N_2O in the atmosphere has been increasing at a rate of about 0.2% per year and is the tenth most abundant gas in the atmosphere [10]. NO_2 is also a strong green house gas and is the chemical intermediate prior to the formation of acid rain in the atmosphere for oxidized nitrogen [11].

Table 1 **Summary of the several side reactions in SCR chemistry (reproduced from [12])**

Other reactions over the SCR catalyst affect performance

Reaction/comments	Condition
Oxidation of NH_3 uses NH_3 increases NO_x	high temperature extremely low NO_x
Nitrous oxide (N_2O) formation	type of catalyst absence of moisture
Nitrite/nitrate salt formation explosive	low temperature
Ammonium (bi)sulfate condensation plugging particulates	catalyst composition SO_2 oxidation to SO_3 low temperature

1.1.3 Catalytic DeNO$_x$

Several catalytic technologies have been developed to facilitate the SCR reaction. The general performance of these catalysts are shown in Figure 2.

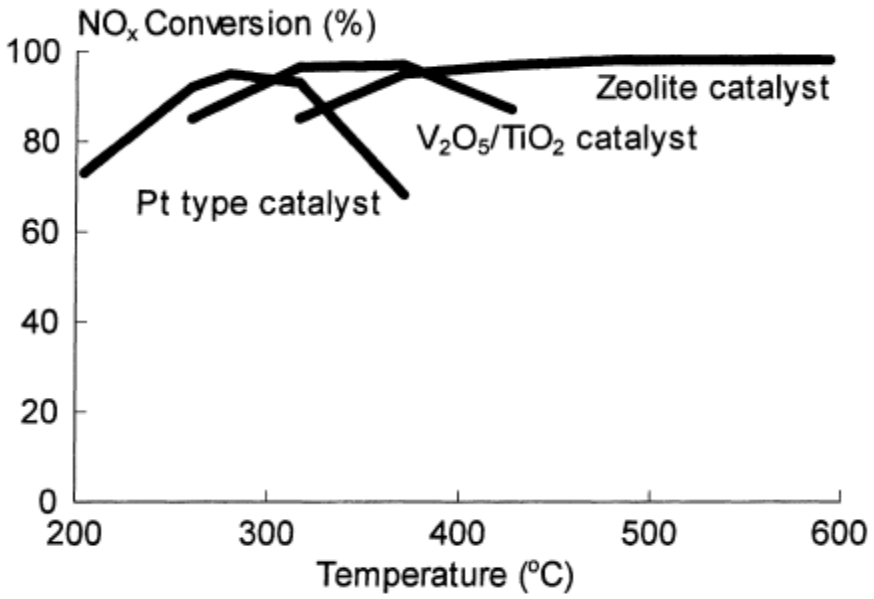

Figure 2 **General NO_x conversion trend of different SCR catalytic technologies (reproduced from [12]).**

The first catalyst widely used in commercial applications was the vanadium oxide catalyst but recently zeolite catalysts have become more popular. The zeolite catalysts have shown the best NO_x conversion at high temperatures; they are also tolerant to other contaminates that may be present in fossil fuel combustion streams like sulfur oxide compounds (SO_x) [12]. Typically these catalysts have been used in stationary industrial applications which require a cheap catalyst that can handle large volumes of exhaust gas streams. This work however will focus on low temperature precious metal technologies for automotive applications. As was mentioned in section 1.1.1. this is becoming an increasingly attractive technology because of increased federal requirements. This technology would have to utilize an additional storage tank and injection system in order to introduce the reductant to the system that could be stored in the form of urea. Urea is an aqueous solution at ambient

pressures and temperatures. When the urea is introduced to a hot exhaust gas stream it decomposes into ammonia and isocyanic acid, the latter hydrolyzes to innocuous species almost immediately which leaves ammonia as the active reductant [3].

Platinum has been shown to give high selective conversion of NO_x at low temperatures [12] and cobalt supported on γ-Al_2O_3 has also been shown to yield high SCR activity by itself [13]. This work will investigate these two metals and also investigate using both of these metals in tandem to increase SCR activity. Furthermore, while there is an abundance of information in the literature regarding the SCR actively of several precious metals such as platinum, palladium, and rhodium there has not been much work done with ruthenium which this work will also investigate.

1.2 Reverse Micelle Synthesis

Mircoemulsion solutions are isotropic, thermodynamically stable solutions consisting of two immiscible components and amphiphilic components called surfactants. The nature of the microemulsion depends on the relative concentrations of each component. In the case of reverse micelles, the relative amount of oil to water is large. Water droplets are stabilized by the surfactant within a larger oil phase. By selecting metal salts that only dissociate in water, the suspended water pools provide a microenviroment for the preparation of metal nanoparticles [14].

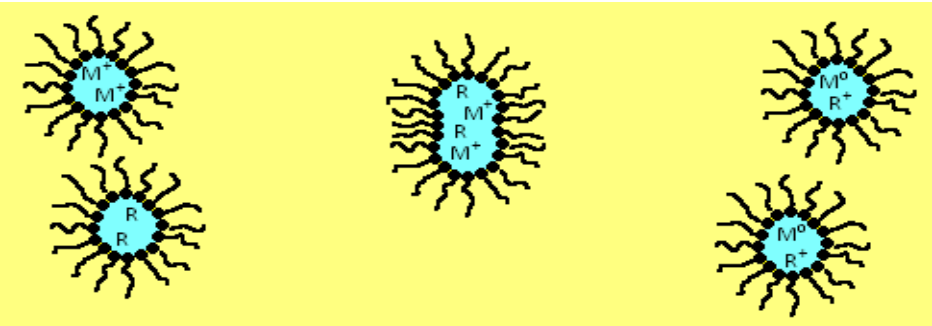

Figure 3 **The surfactant stabilized the water (white) which contains the metal and reductant in the oil phase (yellow) (reproduced from [4]).**

Water-in-oil (w/o) microemulsions were first used to synthesize catalytic particles by Gault in collaboration with Friberg in 1982. The common method for metal nanoparticle synthesis during that time, which is still employed today, was the impregnation method. This method is a simple, scalable technique that allows for the creation of nano-sized particles, but it is difficult to obtain a narrow particle size distribution. With impregnation it is also difficult to control the interaction between two or more metals due to the morphology of the catalytic support when bimetallic or trimetallic particles are the desired outcome. Microemulsions have been proven to be a suitable environment to create nanoparticles with narrow size distributions as well as to control the composition of bimetallic particles due to the microemulsions' specific, well defined structure [15].

1.2.1 Variable Parameters of Microemulsion Synthesis

Several tunable variables are involved in the complex synthesis of microemulsion solutions, all of which affect the size of the reverse micelles and the size of the

resulting nanoparticles. Furthermore, several different combinations of these variables have been shown to yield nanoparticles.

1.2.1.1 Water to Surfactant Ratio

The ratio of the concentration of water to the concentration of surfactant, ω , in the microemulsion solution controls the size of the micro-sized water pools. If the amount of surfactant in the solution in increased while holding the concentration of water constant it will increase the number of water droplets [15]. This will also decrease the number of metal atoms per water droplet and consequently the size or the metal particle. Pileni et. al. has shown that the that dependence of water droplet radius on the water-to-surfactant ratio yields a linear relationship [16].

1.2.1.2 Nature of the Reductant

The amount of reductant relative to the moles of metal has also shown to influence particle size; increasing the amount of reductant while holding the moles of metal salt constant will decrease the size of the particles. Chen et. al. has displayed this trend with Ni particles prepared in a microemulsion containing cetyltriammonium bromide (CTAB) as the surfactant, hydrazine as the reductant, *n*-hexanol and water at a temperature of 73°C. Moreover, the diameter of the particle reaches a minimum value when the ratio of reductant to metals moles is above 10 [15].

1.2.1.3 Influence of the Surfactant on Microemulsion Solutions

The formation of metal particles ultimately depends on the ability of the surfactant to sterically stabilize the micro-sized water pool to allow the metal salts to interact with the reductant and other metal particles. The formation occurs in two steps, first the metal is reduced and particles begin to nucleate and grow. Since the solutions are stirred there are constantly collisions between the reverse micelles which cause the formation of dimers as depicted in the following figure. The reverse micelles can exchange contents before decoalescence through molecular diffusion which leads to reaction and nucleation which increases the size of the metal particles as shown in Figure 4.

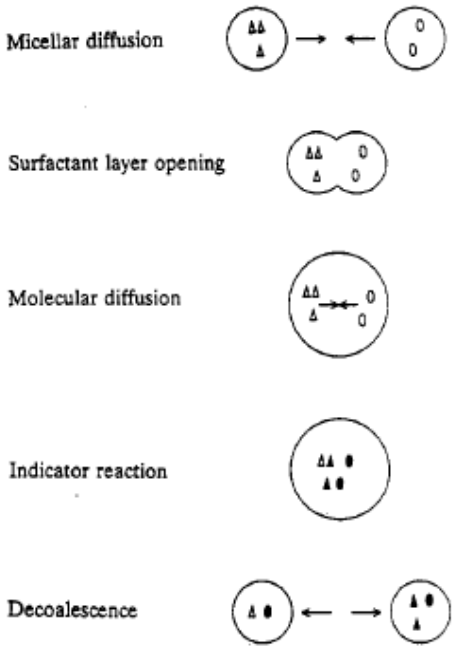

Figure 4 **A schematic of the five elementary steps associated with reverse micellar coalescence, solubilizate exchange, reaction and decoalescence. (reproduced from [4])**

1.2.2 Preparation of Supported Catalytic Particles from Microemulsion Solutions

Since the reverse micelles are inherently stable it is hard to liberate the metal nanoparticles from the suspension without the addition of another substance. Sources in the literature add a polar solvent such as acetone or tetrahydrofuran (THF) to disrupt the microemulsion. The solvent will compete with and displace the adsorbed surfactant molecules allowing for sedimentation of the nanoparticles. If this process is carried out under proper mixing conditions in the presence of a powder support, a homogeneous distribution of particles on the support surface can be obtained. The supported nanoparticles are then calcined at elevated temperatures (typically above 500 ºC) to remove any residual surfactant [4].

Chapter 2

Experimental

2.1 Materials

Ruthenium (III) chloride, anhydrous and cobalt (II) chloride, hexahydrate (98+%) were purchased from Strem Chemicals Inc. and kept at room temperature. Both chloroplatinic acid, hexahydrate (ACS reagent) and barium nitrate (Puratronic® 99.999% metal basis) were kept in a vacuum desiccator prior to use and purchased from Sigma-Aldrich and Alfa Aesar respectively. Catalox® Sba-200 Alumina (γ-Al_2O_3) was used as the support for all catalysts in this work.

Certified ACS reagent grade cyclohexane and 2-propanol were purchased from Fisher Scientific; Brij® 30 and hydrazine hydrate were obtained from Sigma-Aldrich; and Triton X-100 was purchased from Alfa Aesar.

The gas cylinders used in this work were as follows: a 2000 ppm nitrogen oxide cylinder balanced with nitrogen purchased from Matheson Tri-Gas, a 2000 ppm ammonia cylinder balanced with nitrogen also purchased from Matheson Tri-Gas, a research grade carbon monoxide cylinder purchased from Matheson Tri-Gas, and industrial grade nitrogen and oxygen cylinders both purchased from Keen Compressed Gas Co.

2.2 Nanoparticle Synthesis

The monometallic Pt and Ru nanoparticles were reduced in reverse micellar solutions with hydrazine using two different micellar chemistries. The numbers and methods for the Brij® 30 chemistry was adapted from Vijay [17] and Rogers [4]. In these works the metal molarity was 0.1 M, the reductant to metal molar ratio was 1:15, the Brij® 30 concentration in water was set to 0.1 M, and ω was set to 3 where ω is

$$\omega = \frac{[water]}{[surfactant] + [cosurfactant]}.$$

The second chemistry used involved Triton X-100 and was adapted from Zhang et. al. [18]. Zhang used 2-propanol as a co-surfactant, therefore the amounts of Triton X-100 and 2-propanol were added together in the calculation of the water to surfactant ratio as described above. In Zhang's paper the metal molarity was 0.04 M, the reductant to metal molar ratio was 1:7.5, the surfactant concentration was calculated to be 0.015 M from volume fractions of the reagents given by Zhang, and ω was set to 1.3.

In both chemistries the metals were first dissolved in de-ionized water with a fixed metal concentration. Simultaneously a solution of hydrazine and water was created in a second vessel with a fixed ratio of reductant concentration to metal concentration. Once the metals and reductants were completely dissolved cyclohexane was added to each solution causing the solutions to phase separate into an aqueous solution and an oil phase. Then the surfactant, which was either Brij® 30 or Triton X-100 with the addition of a co-surfactant, 2-propanol, was added to both of these solutions to satisfy ω.

These solutions were left to stir for at least an hour. If optical clarity, indicating the formation of micelles, was not obtained after this hour either more Brij® 30 or 2-

propanol, depending on which was previously present in solution, was added drop wise until optical clarity was obtained.

After the metal and reductant solutions were left to stir for an hour the two vessels were mixed. The solutions containing Pt exhibited a color change from green to purple when the reductant solution was added, indicating reduction of the metal. No color change was observed for the Ru reverse micelle solutions because the solution before and after reduction was opaque and black. The metal and reductant solutions were allowed to stir for at least twelve hours before anything further was done to solutions.

2.3 Supported Catalyst Synthesis

The catalysts were named by stating the each percent weight loading of the metal followed by its atomic symbol (e.g. 1Pt5Co15Ba was 1, 5, and 15 w/w% of platinum, cobalt, and barium respectively). The balance of all catalysts was the γ-Al_2O_3 support.

After the reverse micellar suspended metal nanoparticles were allowed to stir and reduce in solution for at least twelve hours γ-Al_2O_3 support was added to the solution along with twice the solution's volume of acetone which was added dropwise. The actone was implemented to break the micelles and force the metal nanoparticles to fall out of solution and interact with the support. When the dropwise addition of acetone was complete the solution was removed from the stirrer and the catalyst was allowed settle to the bottom of the vessel leaving a clear supernatant above it which was siphoned off. The catalyst was then washed with acetone to remove surfactant and unwanted material away from the catalyst using a vapor venting wash bottle. The same settling and siphoning procedure was then repeated. Next the wet solids were poured through a Whatman® Filter (Cat. No. 1001-042) under

suction. The filter was then dried at 100°C for two hours or until the catalyst can be scraped off.

The PtCoBa and RuCoBa catalyst were synthesized by incipient wetness technique. For these catalysts the appropriate amount of metal was dissolved in the minimum amount of de-ionized water to get the solution as close to saturation as possible. The solution was then added drop wise to support while stirring to insure uniformity until incipient wetness was reached. The catalyst was then dried for an hour at 100°C. The addition of metal solution to incipient wetness followed by drying was repeated until the entire solution was deposited on the catalyst.

Once both the reverse micelle and incipient wetness catalysts were completely dried under 100°C they were calcined in air in a Fisher Scientific furnace to burn off residual surfactant in the reverse micelle case or to decompose the salts in the incipient wetness case. They were first elevated to 200°C over two hours and then held at that temperature for one hour to remove adsorbed water molecules. The furnace was then raised to 550°C over three hours where they were held for 2 hours. They were then allowed to cool overnight and sealed in a vial until use.

2.4 Analytical Method: High Throughput Experimentation

A 16 channel high-throughput plug flow reactor was used to evaluate the catalytic performance of the catalysts. Each channel had 0.1500 g of crushed catalyst situated in a vertically oriented stainless steel tube (L: 138 mm ID: 4 mm OD: 6 mm) with a 10 μm pore sized Chand Eisenmann Metallurgical Frit. The reactor channels were insulated and heated to the desired temperature; the temperature was monitored using a thermocouple

placed in one of the catalyst beds. Upstream from the catalyst tubes were 16 capillaries to ensure dispersed uniform flow of reactant gases to each channel. The flow of reactant gases were controlled using Brooks 5850 E Series mass flow controllers. A schematic of this setup is shown in Figure 5.

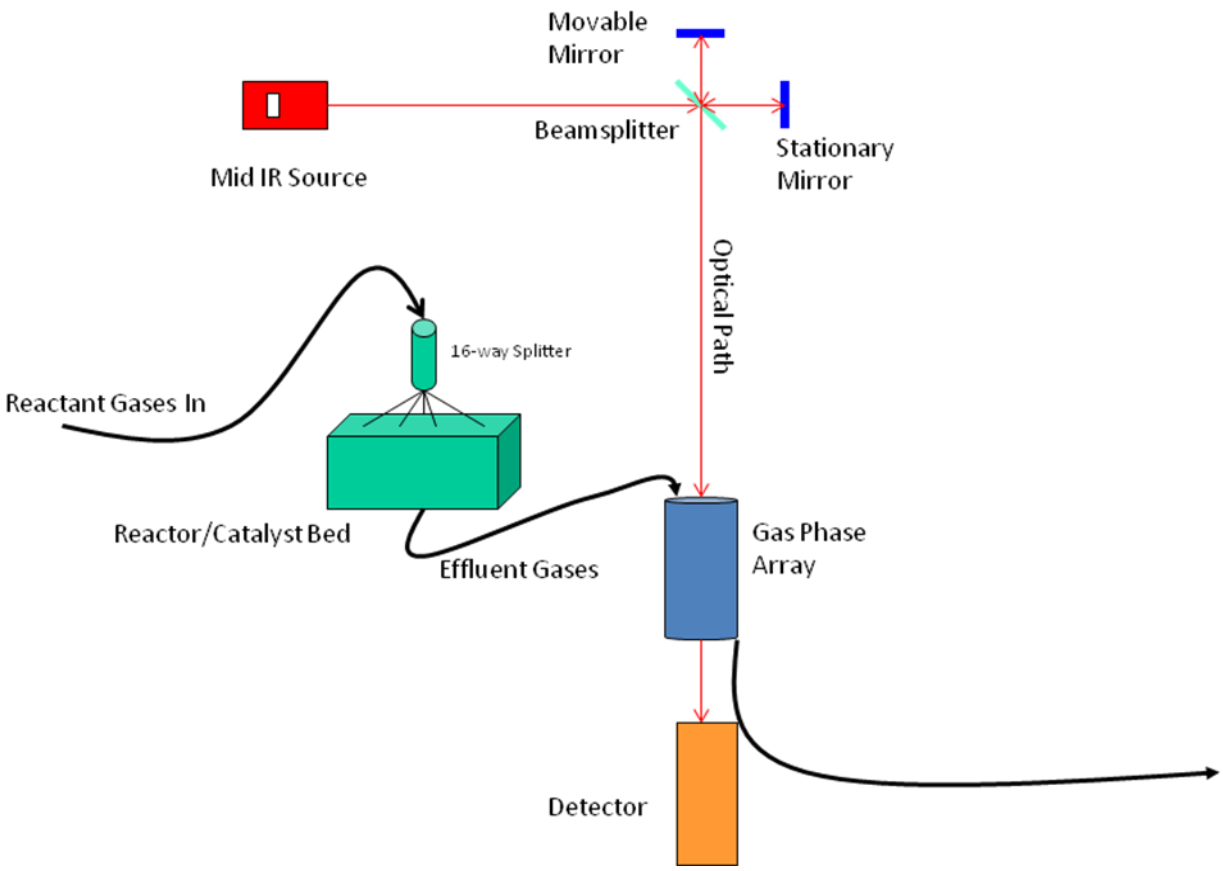

Figure 5 Schematic of High-Throughput Set-up

The effluent gases of the 16 catalytic reactors remained isolated as they were passed through a 16 channel gas phase array (GPA). The GPA provides 16 cylindrical

chambers allowing the effluent gases to flow parallel to an IR beam as depicted in Figure above. Using optics and a Bruker Equinox 55 Interferometer, the IR beam can be propagated through the gases to a 64x64 pixel mercury cadmium telluride focal plane array (FPA) detector (Santa Barbara Focal Plane) where the radiation can be collected and the absorbance of the gases can be analyzed. The GPA contains the gases and the IR beam in such a way that enables parallel analysis while eliminating crosstalk. The instrument is capable of collecting spectral information with a maximum resolution of 0.5 cm-1 over a spectral range from 4000 cm^{-1} to 900 cm^{-1}. A photograph of the GPA is shown in Figure 6 where the red arrows indicate the direction of the IR beam while the blue arrows indicated the flow of effluent gases from the catalyst beds.

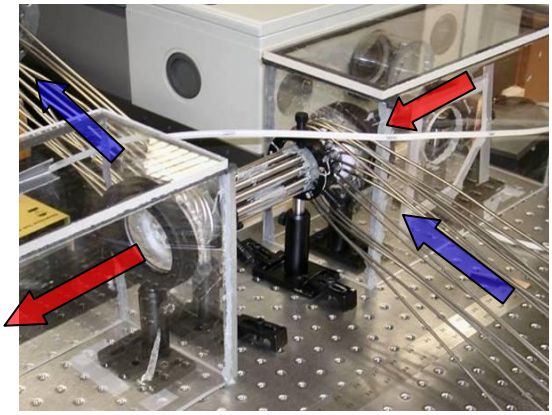

Figure 6 **Photograph of the GPA. The red arrows indicate the direction of the IR beam while the blue arrows indicated the flow of effluent gases from the catalyst beds (reproduced from [17]).**

The detector was controlled using WinIR software and the data was processed using software created in house. The raw data was batched processed (remove bad pixels,

Fourier Transformed, calculate absorbance, base-line corrected, and integrate peak height). The end result was NO concentrations at the range of wavelengths as a function of temperature.

2.4.1. NO and NO_2 Calibration

Univariate calibrations were conducted for both NO and NO_2 and were used to quantify the IR transmission data for the high-throughput SCR experiments. Beer's Law gives a relationship between concentration and absorbance at a given wavenumber by the following:

$$A(\bar{v}) = a(\bar{v})bc$$

Where $A(\bar{v})$ is the absorbance as a function of wavenumber, $a(\bar{v})$ is the absorptivity constant, b is the path length, and c is the concentration. The peak height or integrated peak are is linear with the absorbance at low concentrations at a given wavenumber or range of wavenumbers respectively. Due to this linear relationship the data can be calibrated [19].

The following linear calibrations were completed by flowing a known amount of NO or NO_2 through the experimental set-up described previously at room temperature over through empty reactor tubes. The NO_x gases were balanced with N_2 in order keep the pressure in the system constant.

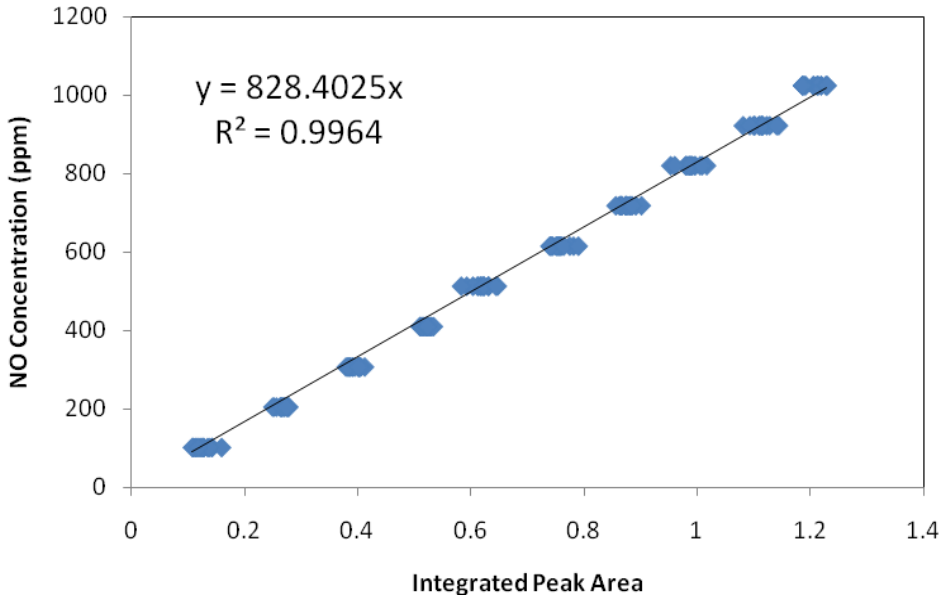

Figure 7 **NO Calibration. The peak area of NO was integrated from 1975 to 1800 cm^{-1}**

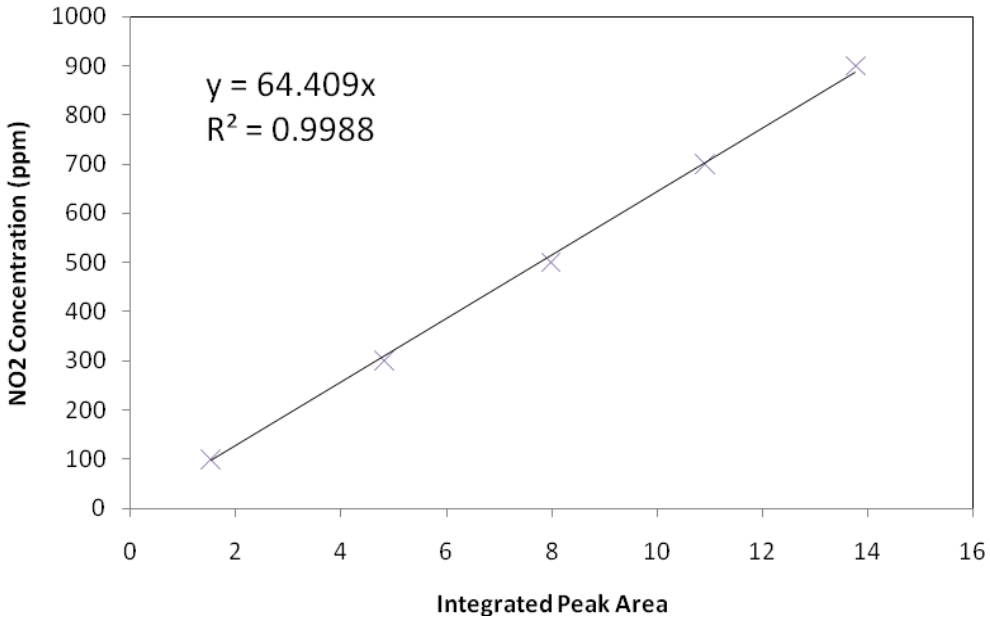

Figure 8 **NO_2 Calibration. The peak area of NO_2 was integrated from 1660 to 1540 cm^{-1}**

2.6 Characterization

An Altamira Instruments AMI-200ip was used to perform pulse chemisorption experiments to determine the percent dispersion of catalysts. 0.1 g of catalyst was placed in a glass u-shaped tube and plugged with quartz wool. The glass tube was placed in an insulated furnace and attached to reactant gases. The catalysts were heated to 450 °C at 10 °C/min and 45 sccm of hydrogen was flowed over the catalyst for an hour to pretreat the catalysts. Then 40 individual pulses of 58 µL of CO at 30 sccm were sent over the catalysts in the presence of helium. In order to calibrate the data, 10 pulses of CO at 30 sccm were sent through a null cell in the system. A thermal conductivity detector was used to determine the amount of CO that

was present in the gas stream after it was pulsed over the catalyst. Helium was used since its thermal conductivity is sufficiently different then that of CO. From the ratio of the calibration peak area and the experimental peak area the uptake of CO can be determined. From the weight of catalyst and stoichiometric ratio of the metal with CO adsorption (a value of 1 and 0.6 was used for platinum and ruthenium respectively) the percent dispersion was be calculated using the CO uptake data.

Chapter 3

INFLUENCE OF SURFACTANT ON 1% REVERSE MICELLE Pt AND Ru CATALYSTS

As described in section 1.2 of this work reverse micelle synthesis has received a lot of attention in the heterogeneous catalysis literature since it has been shown to produce metal nanoparticles with a narrower size distribution and better bimetallic composition control than can ever be obtained with incipient wetness impregnation.

Since 1982 when microemulsions were first used to synthesize catalytic particles several different chemistries using a variety of materials have been shown to yield nanoparticles [15]. The Lauterbach research group has used two different chemistries, each based on a different surfactant molecule. The Brij® 30 chemistry that was used in this work was adapted from Vijay [17] and Rogers [4]. Vijay and Rogers used this chemistry to synthesize Pt-Co and Pt-Rh catalysts respectively and tested them for NO_x Storage and Reduction activity. The Triton X-100 chemistry was adapted from Zhang et. al. [18] who characterized Pt-Co catalysts using transmission electron microscopy (TEM) X-ray diffraction (XRD) and energy dispersive X-ray analysis (EDX). To examine the effect of surfactant molecule this work will use these two chemistries to synthesize 1 % ruthenium and platinum catalysts and test them for SCR activity. The different parameters of these chemistries are described in detail in section 2.2 of this work.

3.1 High Throughput Results

Using the experimental set up described in section 2.4 a 1% Ru reverse micelle catalyst was synthesized using the Triton X-100 chemistry (Ru-X), a 1% Ru reverse micelle catalyst synthesized using the Brij® 30 chemistry (Ru-B), a 1% Pt reverse micelle catalyst synthesized using the Triton X-100 chemistry (Pt-X), and a 1% Pt reverse micelle catalyst synthesized using the Brij® 30 chemistry (Pt-B) were tested for SCR activity. The catalysts were calcined in air for 2 hours at 550 ^{o}C, then reduced *in situ* with 10% hydrogen balanced with nitrogen for 1 hour at 450 ^{o}C to completely reduce the catalysts. They were then cooled down to 50 ^{o}C and 500 ppm of NO, 500 ppm of NH_3 and 10% (v/v) of O_2 in N_2 was flowed over the catalyst at a total space velocity of 822,000 hr^{-1}. An IR spectrum of the reactor effluent was collected after these conditions were maintained for a half hour, representing steady state. After the spectrum was collected, the reactor was heated to 100 ^{o}C. After another half hour, another IR spectrum was collected. This process was continued until data was obtained up to and including 400 ^{o}C. The peak areas for NO, NO_2, and N_2O were integrated from 1975 to 1800, 1660 to 1540, and 2260 to 2180 cm^{-1} respectively.

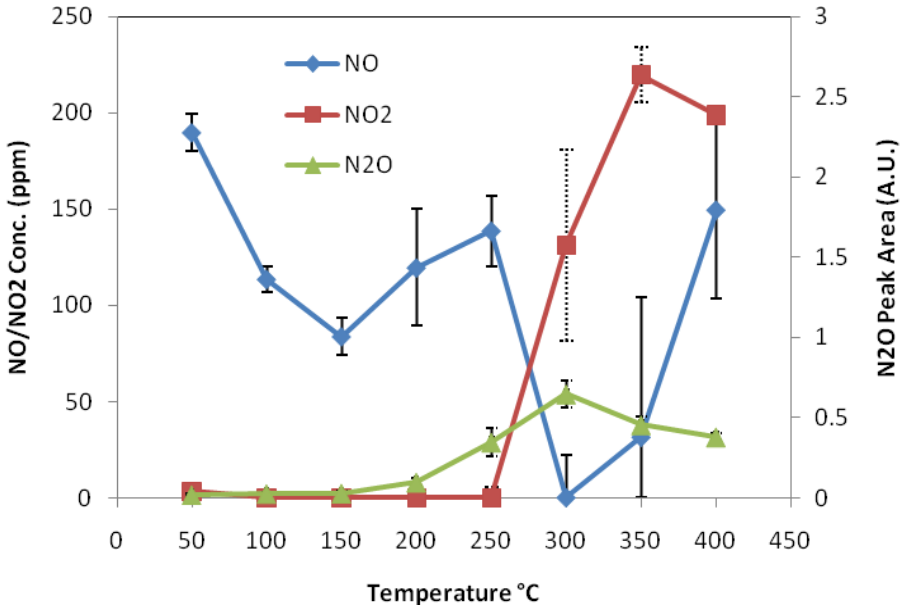

Figure 9 **High-Throughput SCR data for Ru-X catalyst**

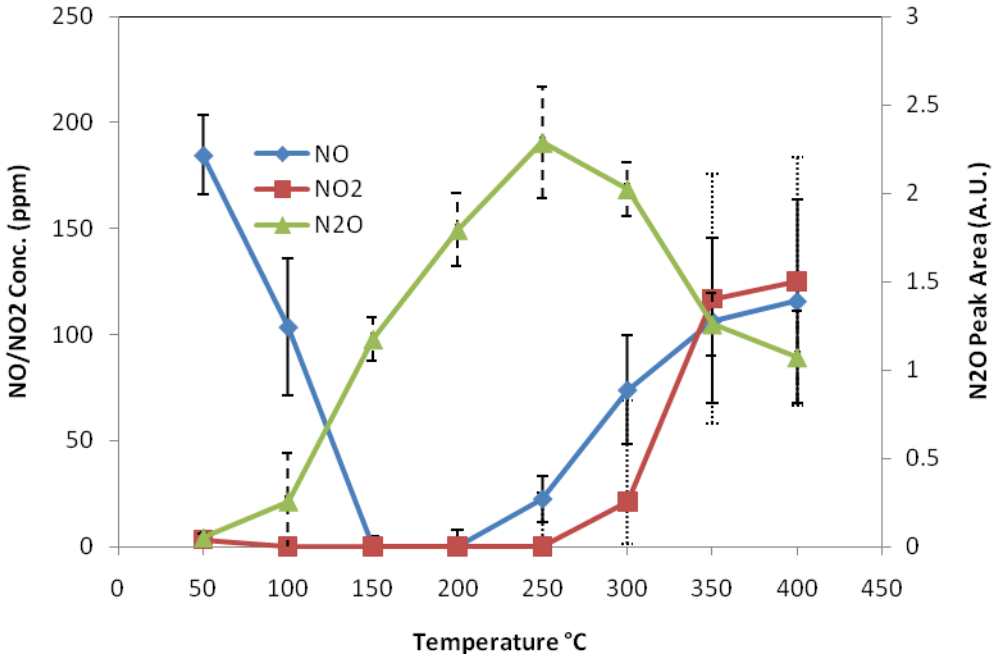

Figure 10 **High-Throughput SCR data for Pt-X catalyst**

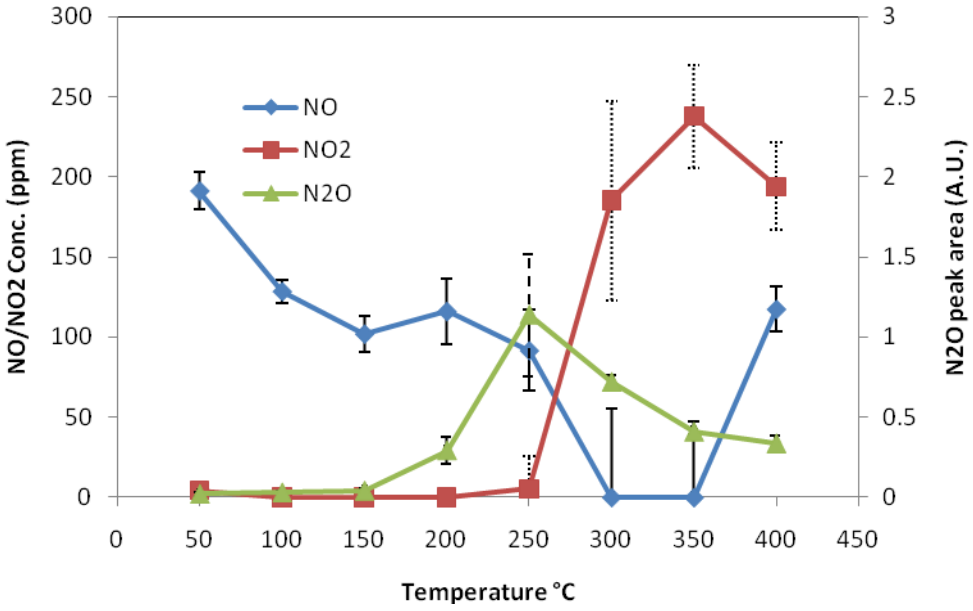

Figure 11 **High-Throughput SCR data for Ru-B catalyst**

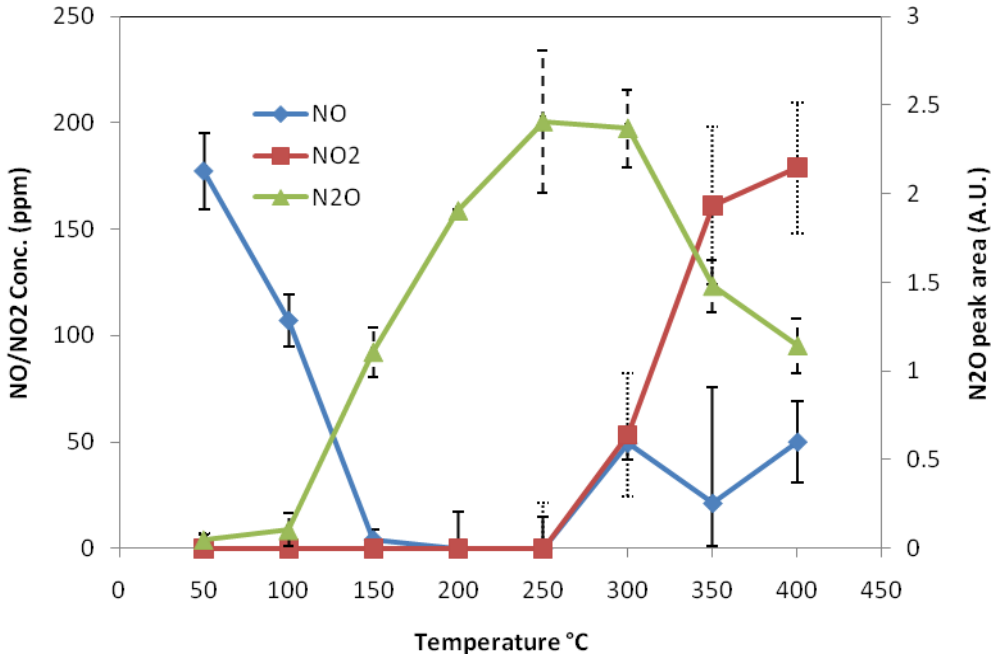

Figure 12 High-Throughput SCR data for Pt-B catalyst

Figures 9-12 show the concentrations of NO, NO_2, and N_2O as a function of temperature for a given catalyst. Prior to this experiment calibrations for NO and NO_2 were conducted in a process described in section 2.4.1. Using these calibrations, peak areas for these species were related to their concentration at each temperature. The left vertical axis describes the concentrations of NO and NO_2. A calibration was not conducted for N_2O because a calibration gas was not available. Therefore, the peak area of the absorbance is reported as displayed on the right vertical axis. It is directly proportional to the concentration of N_2O, and therefore shows the concentration relative to other temperatures.

The NO concentration in Figures 9-12 at 50 ^oC corresponds to a concentration of NO between 250 and 350 ppm even though 500 ppm of NO is flowed over

the catalysts. It was observed that NO conversion occurs over catalysts, pure support, and in empty reactor tubes in temperatures as low as 30 ^{o}C. The extent of this conversion was a strong function of the space velocity and concurrently the pressure system. For example, when a space velocity of 666,000 hr^{-1}, which corresponded to a pressure build up of 31.0 psi upstream from the catalyst, was introduced to the system the initial concentration of NO over Pt-X at 50 ^{o}C was 330 ppm. Conversely, when a space velocity of 822,000 hr^{-1}, which corresponded to a pressure build up of 39.3 psi upstream from the catalyst, was introduced to the system the initial concentration of NO over Pt-X at 50 ^{o}C was 185 ppm. Therefore significant reduction of NO is taking place when NO, NH_3, and O_2 collide in the gas phase.

In each of the four figures above the NO concentration starts out at some high value and then steadily declines with increasing temperatures. At low temperatures, between 50 and 100 ^{o}C the platinum catalysts as exhibited in Figures 10 and 11 show desirable selectivity towards nitrogen, or in other words the yield of NO_2 and N_2O is low. The ruthenium catalysts extend this NO conversion regime out to a temperature of 150 ^{o}C and even at 200 ^{o}C the evolution of N_2O is still very low while the concentration of NO_2 is still close to zero which is displayed in Figures 9 and 12. This NO conversion regime corresponds to reactions 6 and 7 below which were listed in section 1.1.2.

$$6NO + 4NH_3 \rightarrow 5N_2 + 6H_2O \quad (6)$$

$$4NO + 4NH_3 + O_2 \rightarrow 4N_2 + 6H_2O \quad (7)$$

The conversion of NO that is observed at lower temperatures is selective to nitrogen, as evidenced by the lack of N_2O absorbance. As temperatures increase above 200 ^{o}C the concentration of N_2O increases while the concentration of NO continues to fall. Then at

approximately 300 ^{o}C the concentration of N_2O begins to decrease, the concentration of NO_2 begins to increase and the concentration of NO begins to increase. One of the explanations for the increase in NO is ammonia oxidation (catalytic abatement). At high temperatures the oxidation of ammonia increases, which decreases the amount of reductant in the system available to reduce the NO_2 created from NO oxidation to N_2. Instead an increase in NO and NO_2 is observed. These three NO conversion regimes were observed for all the catalysts studied in the work including the Pt/Ru-X/B catalysts.

As can be seen in Figures 9-12 the selectivity of NO conversion towards N_2O is two times higher for the Pt catalysts than the Ru catalysts at the maximum N_2O yield regardless of the surfactant used. The N_2O peak area for the Pt catalysts reach values of 2.3 and 2.4 absorbance units (A.U.) while the Ru catalysts yield maximum N_2O peak areas of 0.6 and 1.1 A.U. This occurred at temperatures between 150 and 250 ^{o}C. Conversely, the Ru catalysts yield higher selectivity towards NO_2 at temperatures greater than 300 ^{o}C.

Single crystal Pt(111) studies have shown that N_2O should be the expected product in this chemistry. Amorelli et. al. has demonstrated that the hydrogenation is very efficient and facile when oxygen and ammonia are present over Pt at temperatures as low as 295K. This leads to a N(2x2) adlayer that can add itself to NO in a simple radical type reaction [20].

3.2 CO Chemisorption Data

Table 2 and Table 3 show the CO chemisorption data for the Pt and Ru reverse micelle catalysts respectively. In the following tables the % dispersion of the catalyst is defined as the ratio of surface atoms to the atoms in the catalyst particle.

Table 2 CO chemisorption data for the Pt reverse micelle catalysts

	Pt-X	Pt-B
Total Micromoles of CO adsorbed per gram of sample	3.00 ± 0.28	7 ± 4.6
% dispersion	5.9 ± 0.57	14 ± 10.0

Table 3 CO chemisorption data for the Pt reverse micelle catalysts

	Ru-X	Ru-B
Total Micromoles of CO adsorbed per gram of sample	0.90 ± 0.14	1.9 ± 0.57
% dispersion	1.61 ± 0.010	3 ± 1.0

The CO chemisoprtion data above give another insight to the effect of changing the surfacing in the nanoparticle synthesis of these catalysts. The data measure the active surface for CO chemisorption and not for SCR activity but nonetheless yields an additional metric. Furthermore, platinum has a greater ability to chemisorb CO than ruthenium so we cannot use this data to compare the ruthenium catalysts vs. the platinum catalyst but we can use this data to compare the influence of the surfactant on each metal.

As can be seen for both Pt and Ru the Brij-30 surfactant creates more disperse particles which is proportional to catalyst size; higher dispersion corresponds to smaller catalyst size. Therefore, Brij-30 surfactant chemistry yields smaller particles than the Triton-X chemistry for both 1% ruthenium and 1% platinum.

3.3 Transmission Electron Microscope (TEM) Images

Images of the Pt-X and the Pt-B catalysts were taken using dark field transmission electron microscopy by Elizabeth D'Addio. Only 58 Pt-X particles and 56 Pt-B particles were studied but the particles studied were both similar to the other particles of the respective surfactant and unique compared to the particles of the opposite surfactant. Figures 13 and 14 show TEM images of the Pt-B catalyst at scales of 100nm and 50nm respectively.

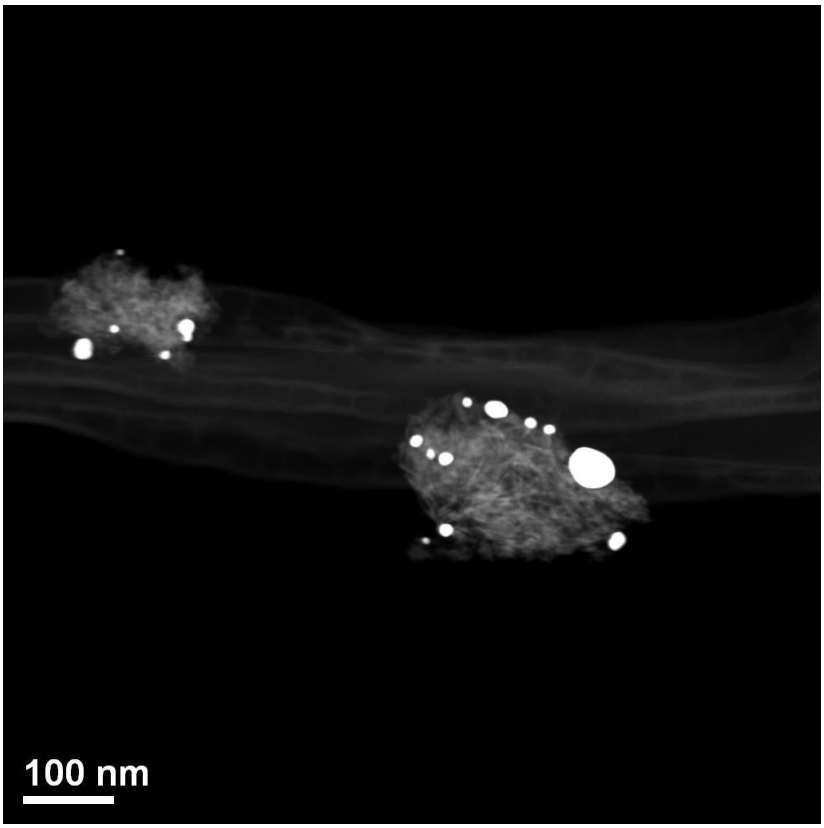

Figure 13 TEM image of Pt-B catalyst at a scale of 100nm

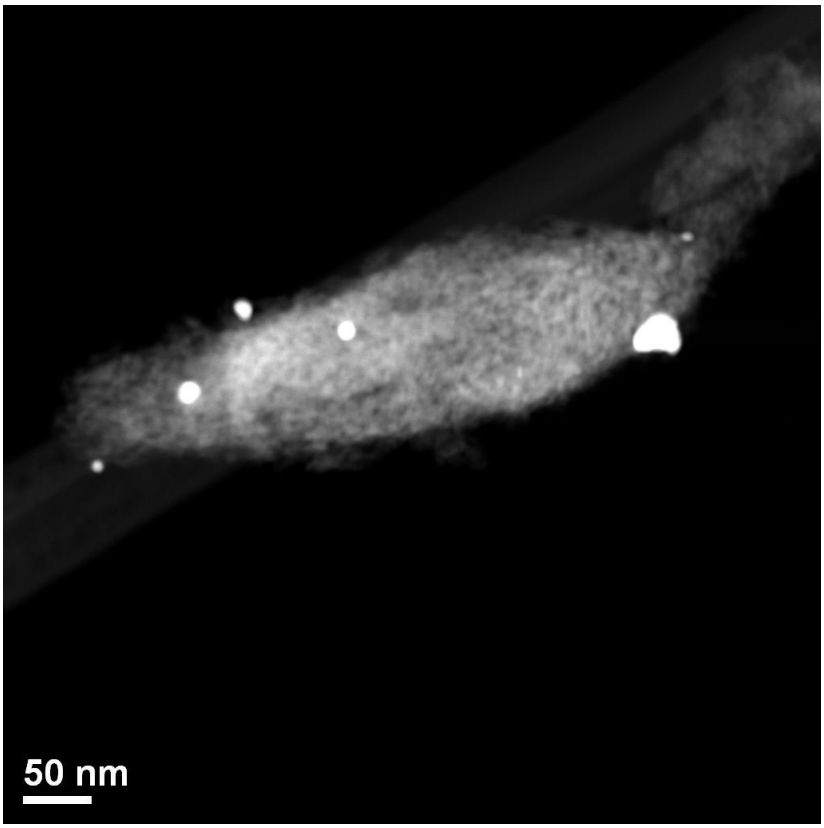

Figure 14 TEM image of Pt-B catalyst at a scale of 50nm

Both of these images show spherical particles that do not appear conglomerated. Conglomeration of the particles decreases the surface area and decreases the ability of the catalysts to perform chemistry. Figures 15 shows TEM image at a scale of 1000nm the Pt-X particles. On average the Pt-X particles appear to be more conglomerated than the Pt-B particles.

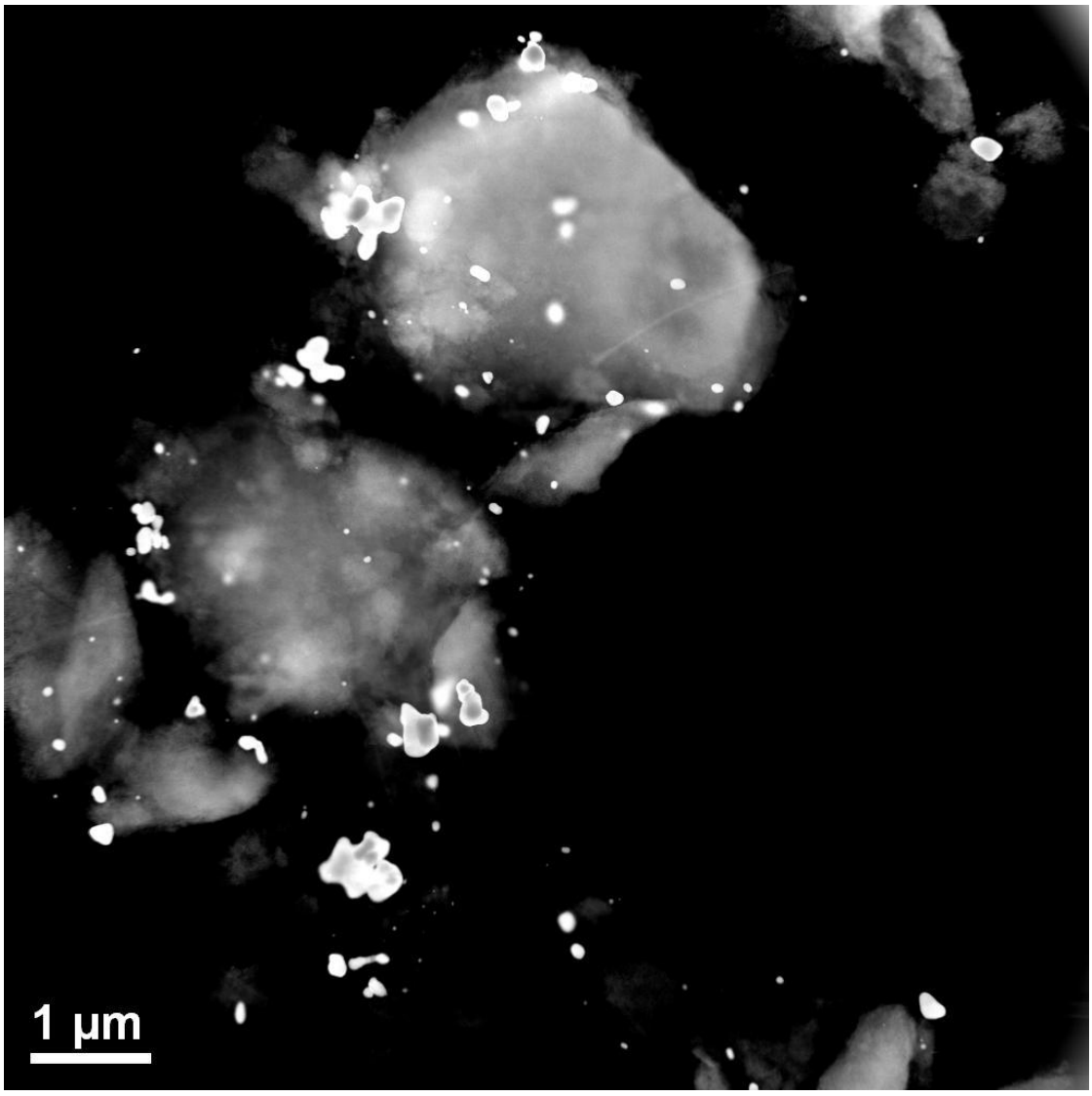

Figure 15 TEM image of Pt-X catalyst at a scale of 1000nm

While the Pt-X particles appear to more conglomerated they were also larger. The Pt-X particles were measured to have an average cross sectional length of 100 ± 69 nm while the Pt-B particles were measured to have an average cross sectional length of 15 ± 10

nm. While these distributions only describe an incredibly small sample of metal they are very different both in span of distribution and average size.

3.4 Conclusions

This section has compared the SCR activity and CO chemisorptions data for 1% Pt and 1% Ru reverse micelle catalysts. Both of these metals were used to produce two different catalysts using a different surfactant and a different surfactant chemistry yielding a total of four catalysts. It was found that the metals yield different results under SCR conditions. The Pt catalysts were able to maintain the conversion of NO close to or at 100% for a longer temperature span than the Ru catalysts and were able to reach 100% conversion at lower temperatures, from 150 to 250^{o}C. The Ru catalysts were not able to reach 100% conversion until temperatures around 300^{o}C, but they were able to achieve a higher selectivity towards N_2 than the Pt catalysts over the entire temperature span studied. The maximum N_2O yields for the Pt catalyst were two times higher than the N_2O yields for the Ru catalysts.

It was also observed that the catalysts synthesized with the Brij-30 performed better than their counterparts synthesized with the Triton-X 100 chemistry. Both the Ru-B and the Pt-B catalysts were able to sustain 100% or close to 100% NO conversion for a longer temperature range than the Ru-X and Pt-X catalysts respectively. The CO chemisorption data also showed that the Brij-30 catalysts had higher CO chemisorption uptake than the Triton-X 100 catalysts. These data were also congruent with the results compiled from the TEM data which showed the Pt-X particles were larger and more conglomerated than the Pt-B particles. Individually these three techniques would not warrant a comment about the ability of each surfactant chemistry to make narrowly dispersed nano-particles. The SCR chemistry is very complicated and has several variables associated with it, the CO chemisorption experiment

can only display correlative data, and the TEM images only showed a fraction of particles. However, the three techniques combined show the Brij-30 catalysts had a lower mean particle size than the Triton-X catalysts and thus was able to obtain higher activity for SCR.

Chapter 4

SCREENING OF RuCoBa INCIPIENT WETNESS CATALYSTS FOR SCR ACTIVITY

After it was shown that 1% Ru and Pt metals displayed SCR activity it was desired to implement other metals and other weight loadings to enhance activity and selectivity. Vijay determined an optimum weight loading for a NSR catalyst at 1% platinum, 5%cobalt, and 15% barium (1Pt5Co15Ba). For the remainder of this work catalysts will be described by their weight loadings and metals as *x*M*y*CozBa, where x, y, and are the weight loadings in percent by mass, M is the precious metal, and Co and Ba correspond to cobalt and barium. In the literature cobalt has been shown to catalyze NO oxidation to NO_2, which subsequently reduces on the alumina surface yielding N_2 which is beneficial for both SCR and NSR chemistries [13]. Barium was used in Vijay's catalyst because of its ability to act as a storage material. It was found that once the NO molecule is oxidized on the catalyst's surface, it then diffuses to a surface barium site where it is stored there as a $*NO_3$ intermediate until it is reduced [17]. This mechanism can also facilitate SCR chemistry. One of the initial goals of this work was to test the 1Pt5Co15Ba catalyst for SCR activity and also investigate the substitution of platinum with ruthenium, which has received little attention in the literature for SCR chemistry, because it is a Pt group metal, and could therefore have similar or better catalytic activity and selectivity.

4.1 SCR activity of 1Pt5Co15Ba vs. 1Ru5Co15Ba

Data similar to those figures presented in section 3.1 were obtained for the 1Pt5Co15Ba vs. 1Ru5Co15Ba incipient wetness catalysts using the same calcination, pretreatment, and experimental procedure described in 3.1. The figures for these two experiments are shown in Figures 16 and 17.

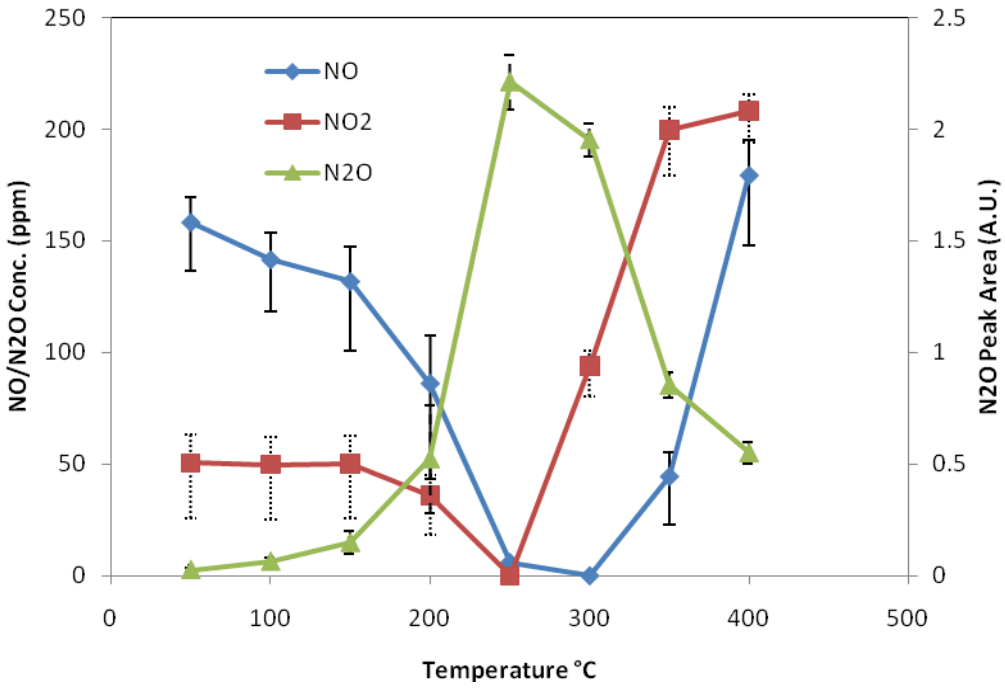

Figure 16 **High-Throughput SCR data for 1Pt5Co15Ba catalyst**

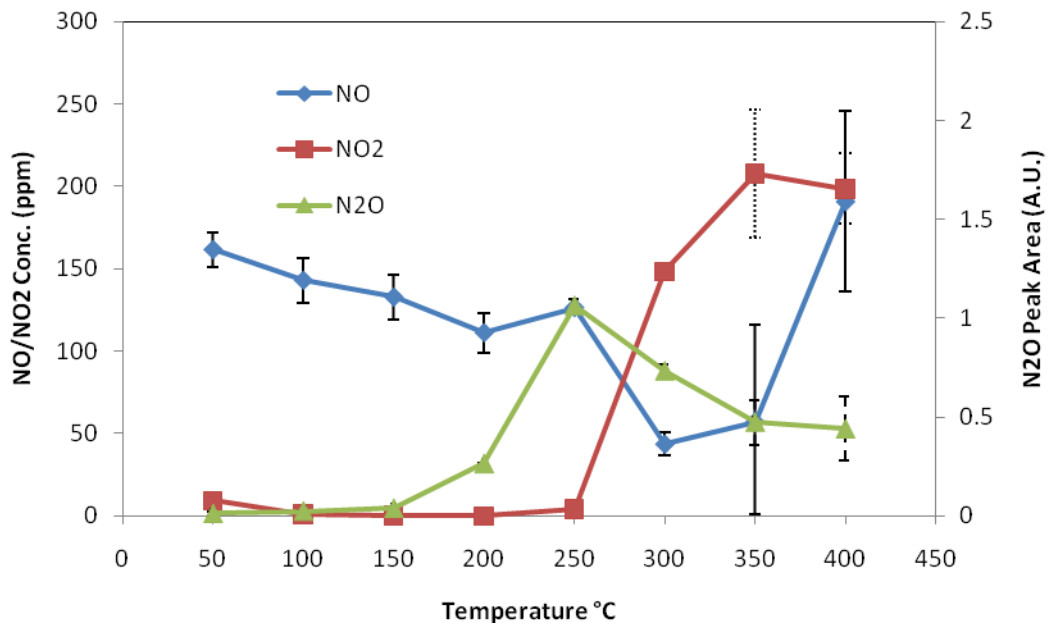

Figure 17 High-Throughput SCR data for 1Ru5Co15Ba catalyst

As can be seen in the previous two figures one can see several similarities between these catalysts and the reverse micelle in regard to the noble metal used. Like the platinum reverse micelle catalyst compared to the ruthenium reverse micelle catalyst, the 1Pt5Co15Ba catalyst shows more selectivity towards nitrous oxide than the 1Ru5Co15Ba catalyst. The N_2O yield reaches a maximum of 2.2 for the 1Pt5Co15Ba catalyst while the yield reaches only 1.1 for the 1Ru5Co15Ba catalyst; a two fold increase just as was observed before. Furthermore the 1Pt5Co15Ba catalyst maximizes NO conversion between 250 and 300 ^{o}C; whereas the 1Ru5Co15Ba catalyst maximizes conversion at slight higher temperatures, between 300 and 350 ^{o}C. Despite these differences the NO_2 yield is nearly identical for these catalysts. Therefore, since the N_2O yield was typically lower for the ruthenium based catalysts than for the platinum based catalyst the next goal of this work was

to achieve optimum weight loadings for the RuCoBa catalyst by varying the amount of ruthenium and cobalt to maximize NO conversion while achieving N_2 selectivity.

4.2 *x*Ru*y*Co15Ba Catalyst Set

In addition to the 1Ru5Co15Ba eight more catalysts were synthesized using incipient wetness. A summary of all nine of these catalysts is shown in Figure 18 and Table 4.

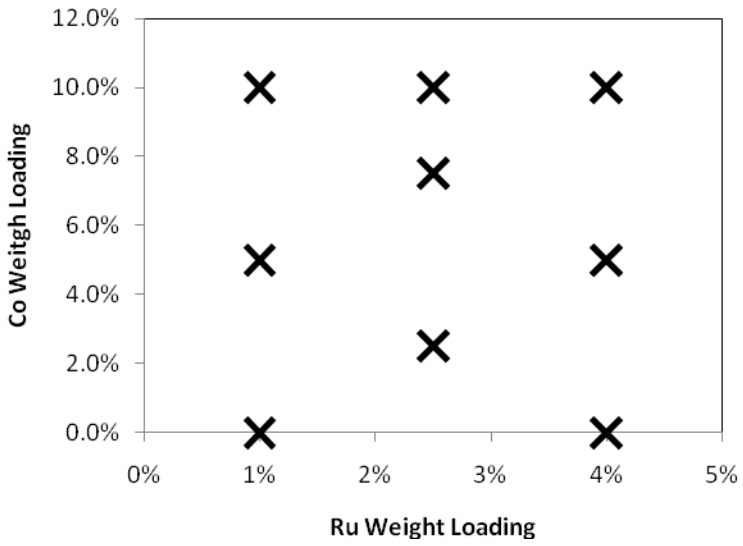

Figure 18 Summary of *x*Ru*y*Co15Ba catalyst library

Table 4 Summary of *x*Ru*y*Co15Ba catalyst library

Catalyst	% Ru	% Co	% Ba
1	1%	5%	15%
2	1%	0%	15%
3	1%	10%	15%
4	2.5%	3%	15%
5	2.5%	8%	15%
6	2.5%	10%	15%
7	4%	0%	15%
8	4%	10%	15%
9	4%	5%	15%

The design of this catalyst library was based on a surface response analysis of the two variants: ruthenium and cobalt weight loadings. The catalyst compositions were chosen to adequately span the parameter space while capturing non-linearity in the relationship between the weight loadings of the two metals.

4.3. High-throughput results for the *x*Ru*y*Co15Ba Catalysts

Using the same experimental procedure that was used to study the other catalysts in this work the additional eight RuCoBa catalysts were tested for SCR activity in the high-throughput reactor. However, for these catalysts the 0.15 g that was packed in the reactor was normalized to the weight loading of ruthenium to keep the moles of precious metal constant. For example when the 4Ru10Co15Ba catalyst was tested 0.15g/4=0.0375g of catalyst was thoroughly mixed with 0.15g-0.0375g=0.1125g of γ-Al_2O_3 and then packed in the reactor tubes to keep the mass of powder, pressure drop across the powder, and the moles of Ru in the catalyst the same. By utilizing this normalization procedure we can determine how the percentage of metal impregnated on a given amount of support changes the formation of the metal particles and thus performance of the catalyst.

Figures 19-21 show the NO, NO_2, and N_2O concentrations respectively as a function of temperature for the 1Ru10Co15Ba, 2.5Ru10Co15Ba, and 4Ru10Co15Ba catalysts. These catalysts have increasing Ru weight loadings and equal Co and Ba weight loadings.

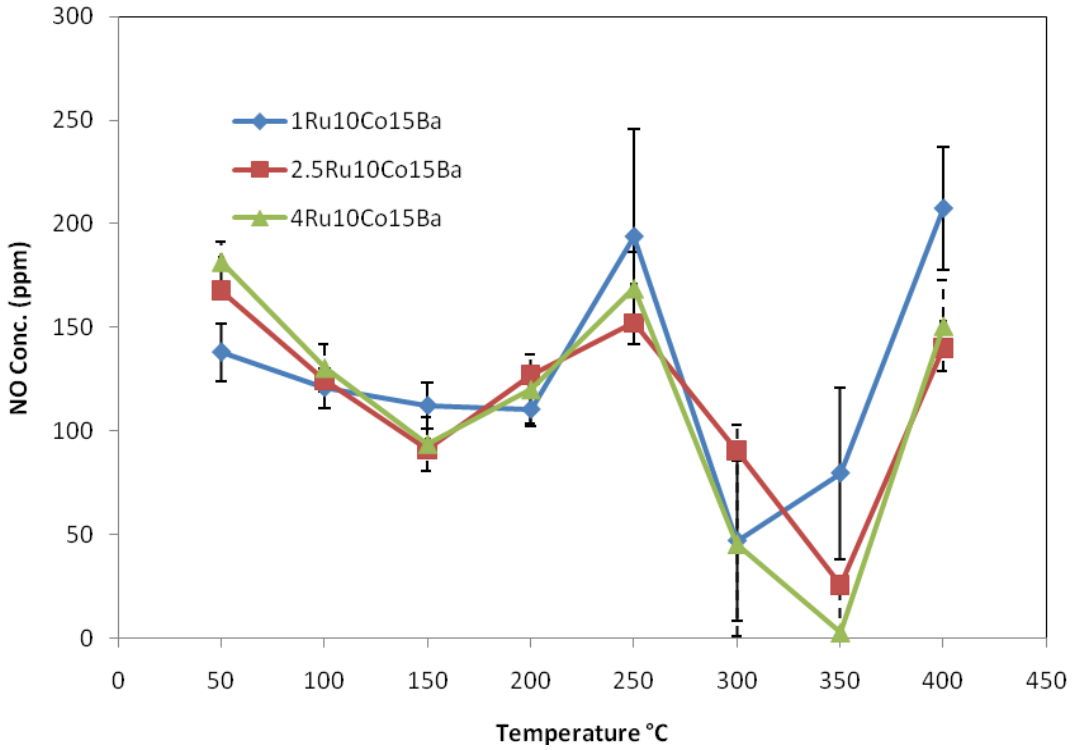

Figure 19 **High-throughput data of NO concentration for the 1Ru10Co15Ba, 2.5Ru10Co15Ba, and 4Ru10Co15Ba catalysts**

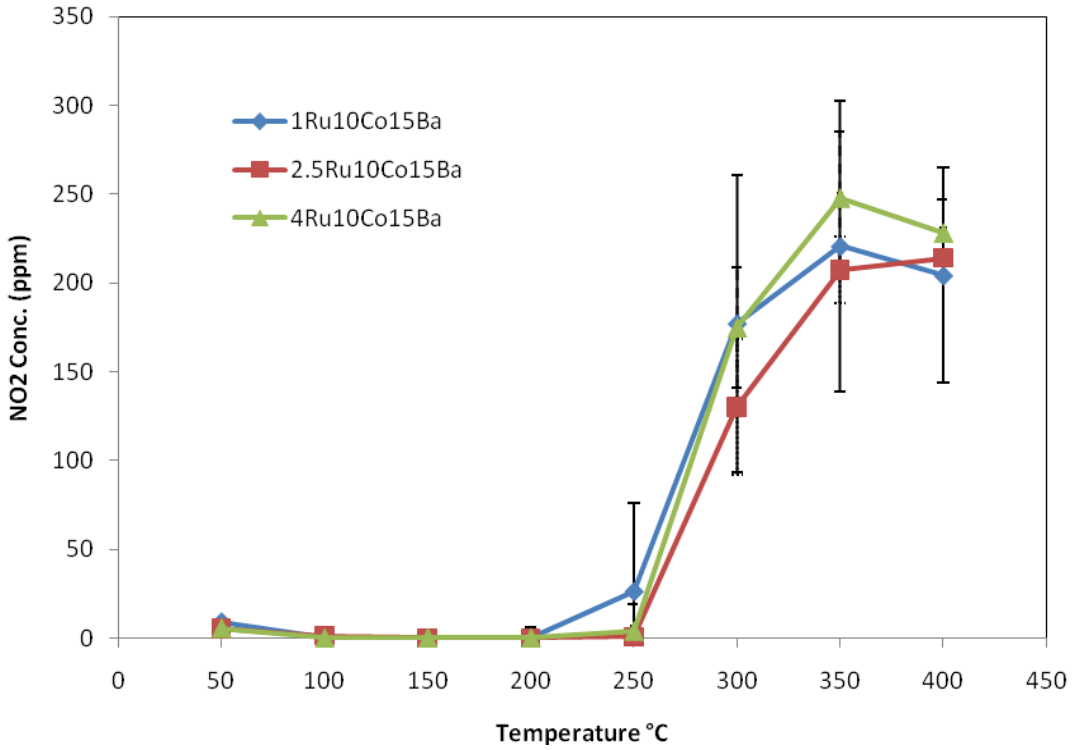

Figure 20 **High-throughput data of NO_2 concentration for the 1Ru10Co15Ba, 2.5Ru10Co15Ba, and 4Ru10Co15Ba catalysts**

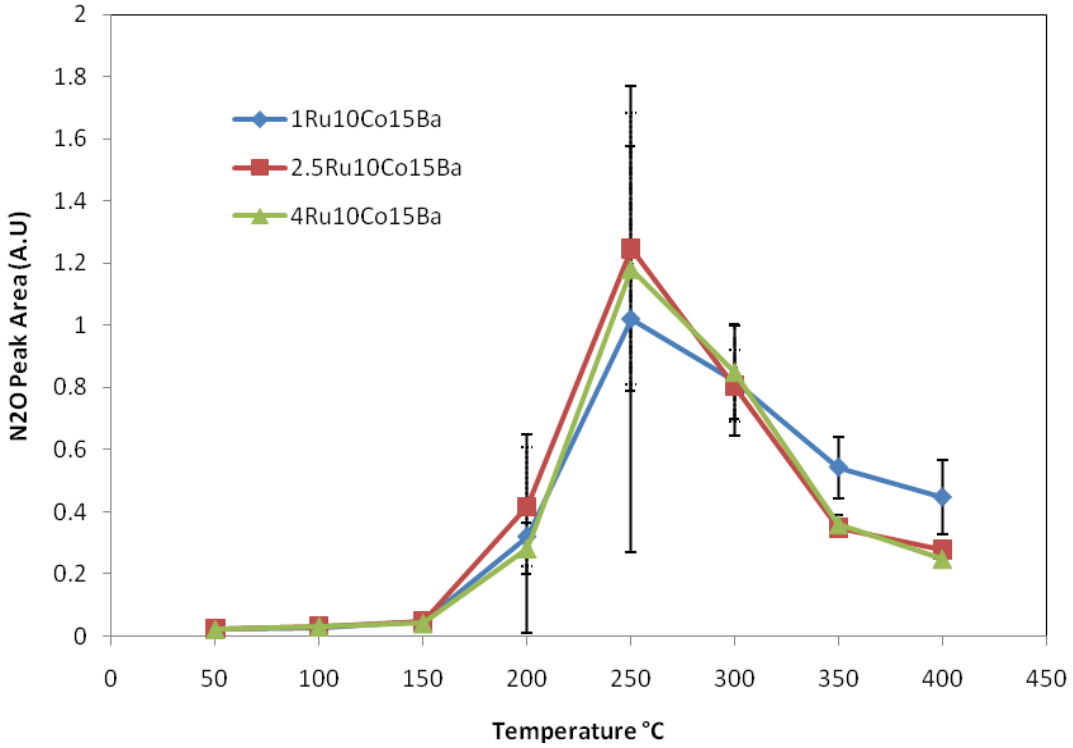

Figure 21 **High-throughput data of N_2O concentration for the 1Ru10Co15Ba, 2.5Ru10Co15Ba, and 4Ru10Co15Ba catalysts**

In Figure 19 the NO concentration as a function of temperature is plotted for the 1Ru10Co15Ba, 2.5Ru10Co15Ba, and 4Ru10Co15Ba catalysts which have an increasing weight loading of ruthenium. The conversion of NO is slightly higher for the 1Ru10Co15Ba at 50 ^{o}C but the NO conversion for the catalysts are not significantly different until a temperature of 300 ^{o}C is reached. At this temperature the 1Ru10Co15Ba converts NO the least and the 4Ru10Co15Ba catalyst performs slightly better than the 2.5Ru10Co15Ba catalyst at 350 ^{o}C. However, it is expected that the influence of increased normalized ruthenium loading would not affect the NO conversions until higher temperatures are reached.

Figures 9-12,16 and 17 showed that the ruthenium catalysts showed their highest NO conversion at temperatures between 300 and 350 ^{o}C . The increased weight loading of ruthenium increases NO conversion slightly at temperatures between 300 and 350 ^{o}C. However this slight increase may not outweigh the benefit of using less ruthenium which is expensive.

As can be seen in Figures 20 and 21 the increased weight loading of ruthenium does yield a slight increase of selectivity towards N_2 and NO_2 rather than N_2O yield at 350 ^{o}C. Figure 20 shows that the concentration of N_2O in the 2.5Ru10Co15Ba and 4Ru10Co15Ba catalysts is slightly lower than the concentration of N_2O in the 1Ru10Co15Ba catalyst at 350 ^{o}C. It also shows that the concentration of N_2O in the 2.5Ru10Co15Ba and 4Ru10Co15Ba catalysts is nearly identical at 350 ^{o}C . However, this is due to the increased conversion of NO at 350 ^{o}C. The ratio of moles of NO that the 4Ru10Co15Ba catalyst converts to N_2 and NO_2 to the moles converted to N_2O is higher for the 4Ru10Co15Ba catalyst than the 2.5Ru10Co15Ba catalyst signifying that the 4Ru10Co15Ba catalyst is more selective to N_2 and NO_2 then N_2O.

Figures 22-24 show the concentrations of NO, NO_2, and N_2O respectively for the 4Ru15Ba, 4Ru5Co15Ba, and 4Ru10Co15Ba catalysts to show the effect of increased Co weight loading with constant weight loadings of Ru and Ba.

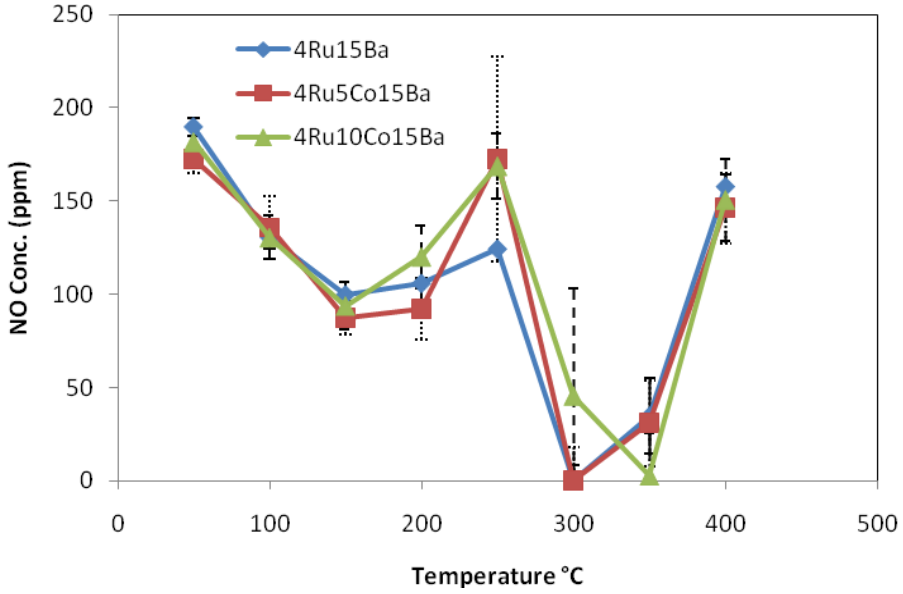

Figure 22 **High-throughput data of NO concentration for the 4Ru15Ba, 4Ru5Co15Ba, and 4Ru10Co15Ba catalysts**

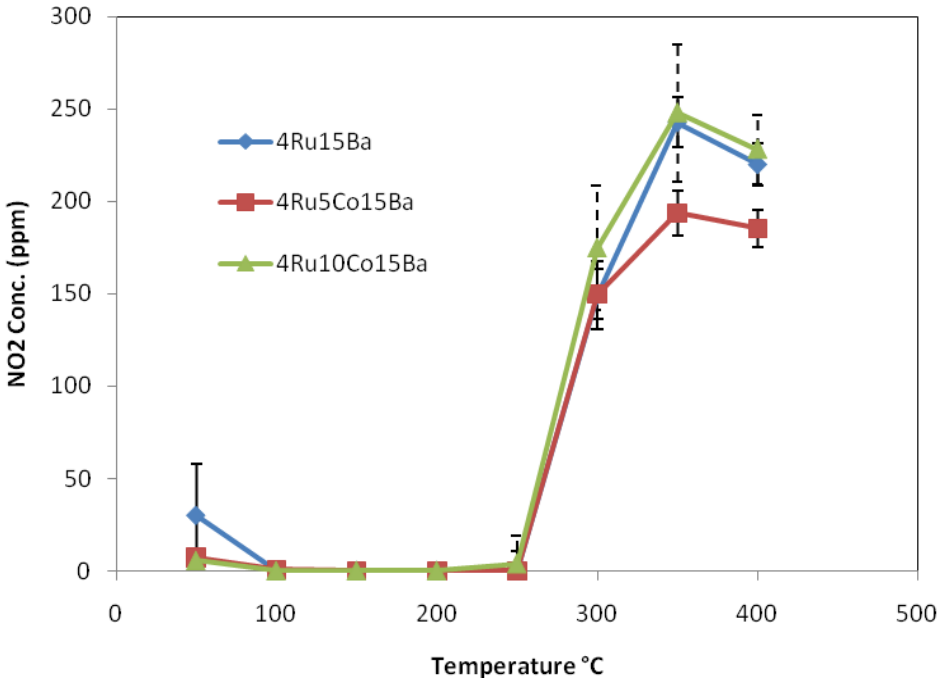

Figure 23 **High-throughput data of NO_2 concentration for the 4Ru15Ba, 4Ru5Co15Ba, and 4Ru10Co15Ba catalysts**

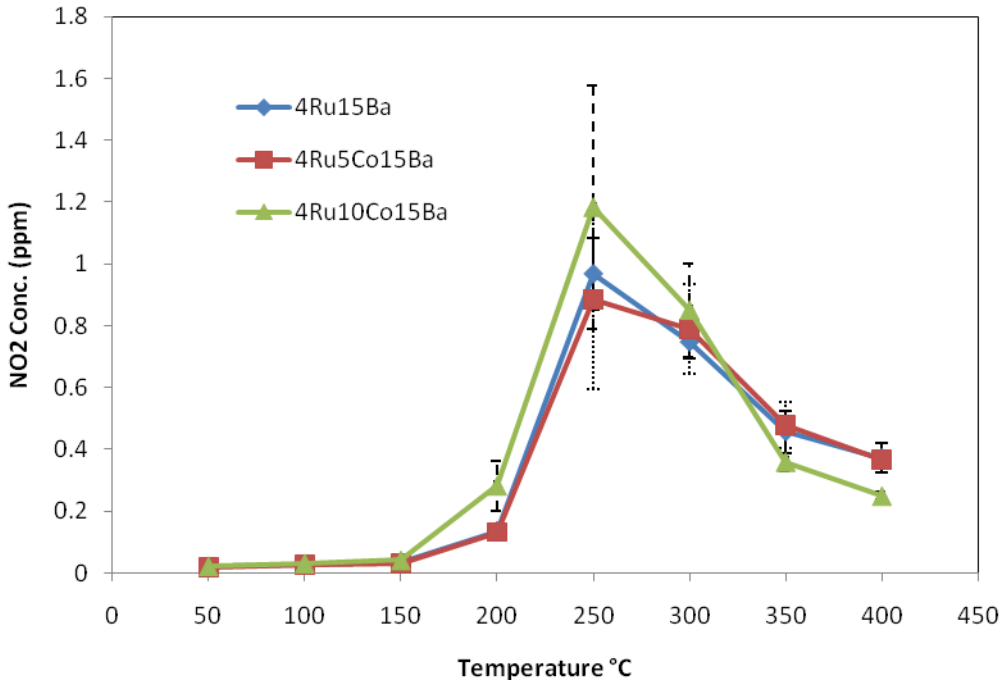

Figure 24 **High-throughput data of N_2O concentration for the 4Ru15Ba, 4Ru5Co15Ba, and 4Ru10Co15Ba catalysts**

Just as was the case with increasing Ru there is little to be said about the improvement of activity and selectivity with changing Co weight loadings. Almost identical NO conversion is observed in Figure 22 and the selectivity towards N_2O is statistically identical in Figure 24. There is a slight improvement in NO_2 selectivity that is observed in Figure 20 for the 4Ru10Co15Ba however no conclusion can be made about the composition of the Ru and Co metals in the catalyst. Perhaps a DFT calculation would be able to give an insight to the ability of Co and Ru in tandem to convert NO in this chemistry but that is beyond the scope of this work.

As was shown in the previous two examples the analysis of this data set is complicated because the reaction conditions can quickly change with temperature due to the nature of the SCR mechanism. It is more beneficial to study all of the catalysts for specific temperatures. Figure 25 shows a 3-dimensional plot summarizing the set of RuCoBa catalysts at 300°C where the numbers of the data points correspond to the catalysts listed in Table 4.

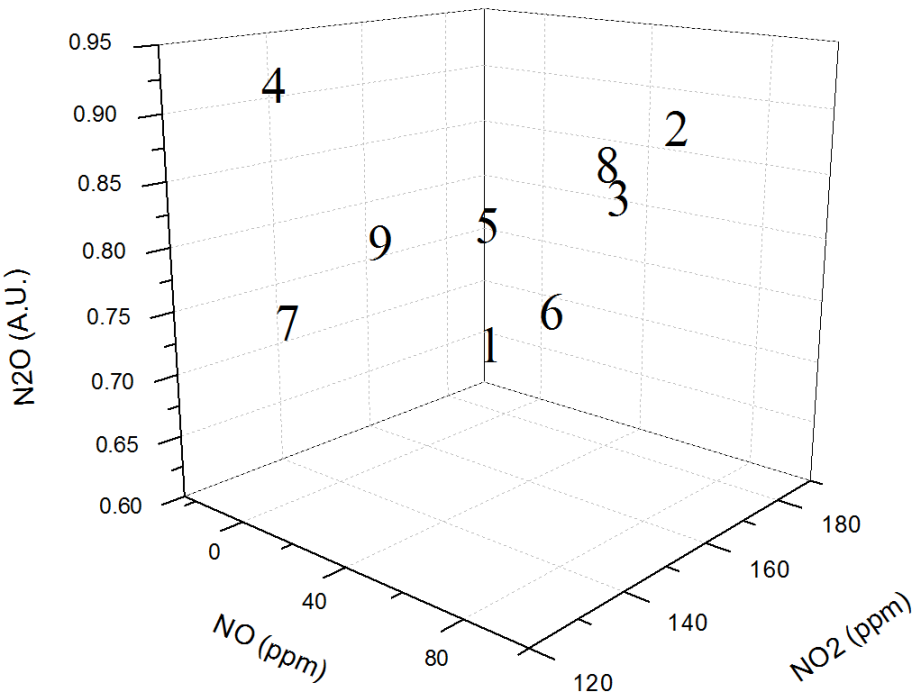

Figure 25 **A 3-dimensional plot of the RuCoBa catalysts displaying the NO, NO_2, and N_2O concentrations at 300°C**

By displaying the data in this fashion activity as well as selectivity can be studied at a given temperature. A catalyst is most active and selective toward nitrogen if is

closest to the lower left most corner which corresponds to the lowest value of all three components.

By inspection of Figure 25 it can be seen catalysts number 7 which is the 4Ru15Ba catalyst performs the best in terms of activity and selectivity. The next best catalysts are numbers 9 and 4 which correspond to the 4Ru5Co15Ba and 2.5Ru2.5Co15Ba catalysts. The worst catalyst at 300^{o}C is catalyst number 2 which is the 1Ru15Ba catalyst. It is not odd that this catalyst performs the worst because it is only one percent metal.

Figure 26 shows the same sets of catalysts at 150 ^{o}C. At this temperature only a 2-dimensional plot is required because in all of the catalysts the concentration of NO_2 is essentially zero.

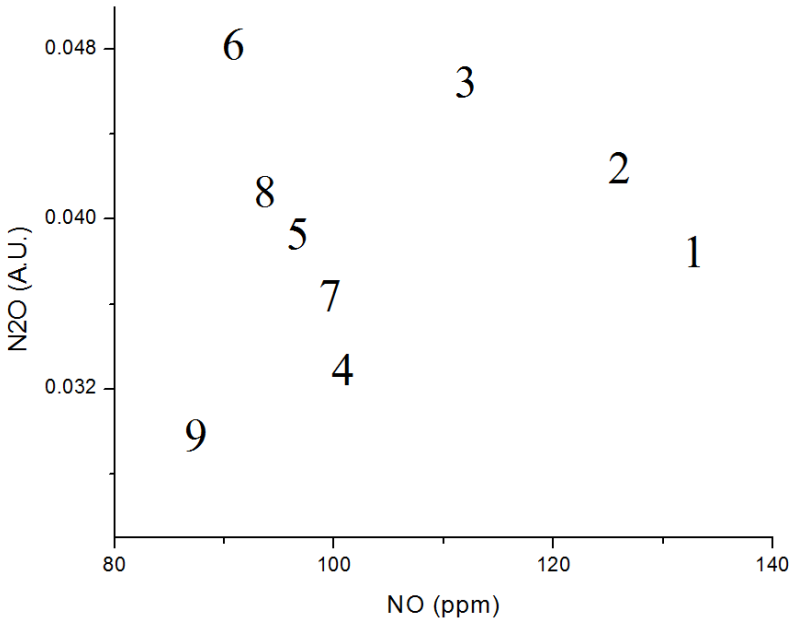

Figure 26 **A 2-dimensional plot of the RuCoBa catalysts displaying the NO and N_2O concentrations at 150^oC**

Again, the catalyst that preformed the best at this temperature is the catalysts closest to the origin showing the highest NO conversion and lowest selectivity away from N_2O. At this temperature 4Ru5Co15Ba catalyst performs the best out of the nine showing more than 90% conversion of NO and creating the lowest concentration of N_2O .

As can be seen in Figures 25 and 26 catalysts 4, 7, and 9 perform the best out of the nine catalysts synthesized at two different temperatures while catalysts numbers 2 and 3 perform the worst.

The last attempt at drawing a conclusion about the influence of Ru and Co was to test a 5Co15Ba catalyst to see if the activity over Co becomes apparent. Figure 27 shows the concentrations of NO, NO_2 and N_2O as a function of temperature for a 5Co15Ba catalyst.

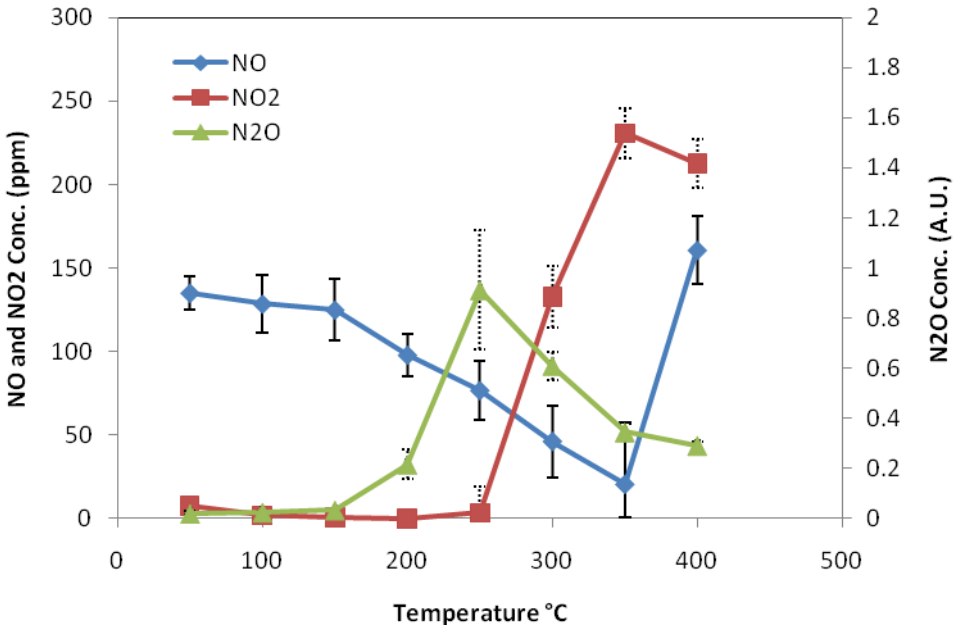

Figure 27 High-Throughput SCR data for 5Co15Ba catalyst

As can be seen in Figure 27 the 5Co15Ba performs comparably well to the other catalysts containing ruthenium. The NO conversion is as high as 95% and the concentration of N_2O never exceeds 1 A.U. which can only be said about the ruthenium catalysts numbers 2, 4, 7, and 9. The one visible downfall to the 5Co15Ba is the large production of NO_2, but it still lies within the range of the other catalyst. However, the production of NO_2 is only

indirectly related to the production of NO_2 which is mainly caused by the deficiency of NH_3 at higher temperatures due to NH_3 oxidation.

In Figures 28 and 29 the 5Co15Ba catalyst was added to Figures 25 and 26 and represented as #10.

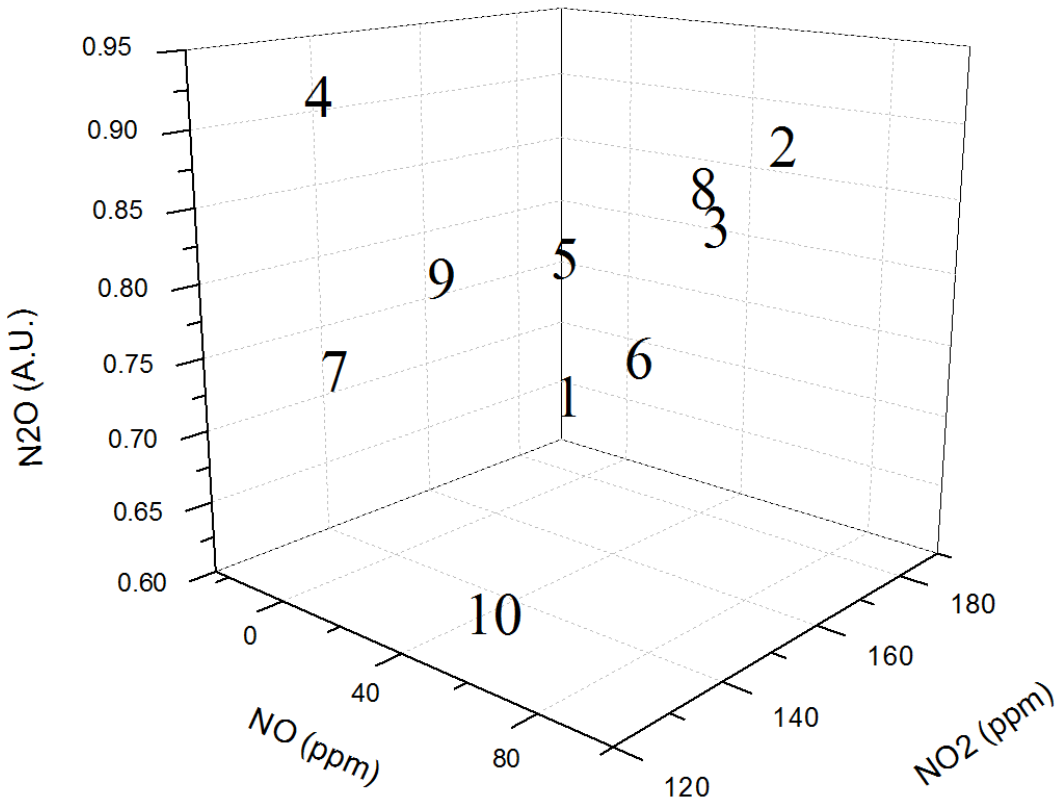

Figure 28 **A 3-dimensional plot of the RuCoBa catalysts displaying the NO, NO_2, and N_2O concentrations at 300°C with the addition of a 5Co15Ba catalyst represented as #10**

At 300 °C it can be seen that the 5Co15Ba catalyst is the most selective catalyst. It can also be seen that #10 does not show very high NO conversion but it still shows higher conversion at 300 °C and across the range of temperatures studied except for the three best: 4, 7, and 9.

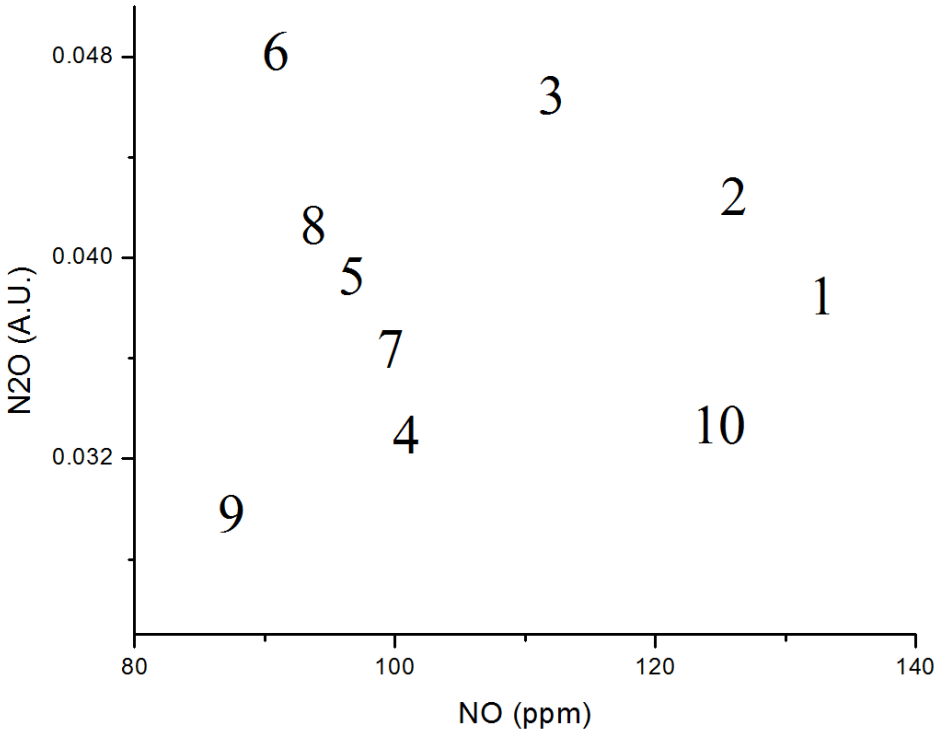

Figure 29 **A 2-dimensional plot of the RuCoBa catalysts displaying the NO and N_2O concentrations at 150°C with the addition of a 5Co15Ba catalyst represented as #10.**

At lower temperatures such as 150°C the 5Co15Ba catalyst is still comparably selective to the RuCoBa catalyst. Even though the catalyst still does not show high NO

conversion it can be clearly seen in Figure 26 that it can yield the same conversion as the 1Ru5Co15Ba and 1Ru15Ba catalysts (#1 and #2 respectively) while still being able to achieve better selectivity than the 1Ru5Co15Ba and 1Ru15Ba catalysts. Therefore, the catalytic activity of the RuCoBa catalysts may be out preformed by a CoBa catalyst if the CoBa weight loading is optimized.

4.4 Conclusion

This part of the work screened a designed set of catalysts for SCR in an attempt to find a relationship between the weight loadings of Ru and Co and the selectivity and activity in the chemistry. First a 1Pt5Co15Ba catalyst, that was previously optimized for NSR chemistry was tested for SCR chemistry and compared to a 1Ru5Co15Ba catalyst. It was observed that the 1Ru5Co15Ba catalyst showed a better selectivity away from N_2O than the 1Pt5Co15Ba catalyst and was able to consume NO better at temperatures greater than 300^oC.

Next a designed set of catalysts was created varying the weight loadings of Ru and Co in an attempt to obtain an optimized catalyst. It was found that the relationship between the metal weight loadings and the SCR activity and selectivity was weak and unsubstantial. However, three catalysts, the 4Ru5Co15Ba, the 4Ru15Ba, and the 2.5Ru2.5Co15Ba performed the best, in terms of activity and selectivity at 150 and 300 ^oC.

It was also observed that a 5Co15Ba catalyst out performed other Ru catalysts with comparable activities in terms of selectivity. Therefore an increased mass of the 5Co15Ba will lead to comparable SCR activity and selectivity as 0.15g of the best Ru catalysts. The increase in mass using the 5Co15Ba catalyst may lead to cost benefits over the

Ru catalysts based on the price of the metals if these catalysts were to be employed in an operating application.

Chapter 5

Future work

More investigation needs to be completed in order to draw a stronger conclusion for the surfactant in the reverse micelle catalysts. Transition or scanning electron microscopy (TEM or SEM) should be done on both the supported catalysts and the microemulsions solutions to enhance the CO chemisorption data. Reverse micelle synthesis is a very effective and simple way to make small laboratory scale catalysts. However, I do not think that it will ever be used on a large industrial scale regardless of the synthesis parameter optimization. This is due to the amount of unrecyclable waste that is created during synthesis. The Brij-30 chemistry requires over 80 mL of cyclohexane to make 1g of 1% (w/w) catalyst. After synthesis this cyclohexane is then completely contaminated by the surfactant which is a strongly adhesive molecule. It is hard to imagine any separation scheme that would be able to effectively separate these two components without causing foaming or a large utility requirement. The Triton-X 100 chemistry requires about 60% less organic solvent but is a far harder molecule to deal with. It is even more adhesive and stubborn than the Brij-30 surfactant; its extreme adhesion to any surface may be the reason why CO and SCR data is worse for the catalysts it synthesizes.

The next step in the high-throughput SCR set-up is to utilize a mass spectrometer to close the nitrogen and oxygen mass balance. Any selectivity relationship in this work was based on comparison because the amount of nitrogen and oxygen molecules exchanged to and from elemental gases could not be detected in the IR.

DFT calculations could be useful in determining a range of Ru and Co weight loading that may be investigated as well as an empirical relationship between the two variables. The span studied in this work did not ultimately capture a trend. Perhaps a more rigorous statistical design would have been able to shed light on the relationship between some variables however without a closed mass balance the data is very convoluted and subject to several variables. In a further optimization the promoter or barium should also be varied.

The applications and SCR technology will to continue grow and be invested in because fossil fuels will still need to be combusted on a large scale for scores of years to come and every technology able to abate pollution from fossil fuels should be utilized and investigated. If used in tandem with another technology that can convert N_2O and/or NO_2 to an innocuous substance can make SCR a very powerful tool. There are also better reductants that can be used and explored to facilitate SCR. For example, if propene is used as a reductant NO_2 creation is far lower than if ammonia is used; but there are still many other problems associated with propene.

References

[1] "Fossil Energy." U.S. Department of Energy. 2010. http://www.fe.doe.gov/.

[2] Wang, Chengjun. Zuo, Yuegang. and Yang, Chen-lu. Selective Catalytic Reduction of NO by NH3 in Flue Gases over a Cu-V/Al2O3 Catalyst at Low Temperature, Journal of Engineering Science, 9 (2009) 26.

[3] Roy, Sounak. Hegde, M.S. Madras, Giridhar. Catalysis for NOx abatement, Applied Energy 86 (2009) 2283–2297.

[4] Rogers, Ben. STRUCTURE AND CATALYTIC PROPERTIES OF ALUMINA-SUPPORTED PLATINUM-RHODIUM BIMETALLIC NANOPARTICLES SYNTHESIZED IN REVERSE MICELLES. Undergraduate Thesis. University of Delaware. 2005.

[5] Tankersley, Jim. Simon, Richard. U.S. to limit greenhouse gas emissions from autos. Los Angeles Times. 19 May 2009.

[6] "Nitrogen Dioxide." U.S. Eviromental Protection Agency. 2010. http://www.epa.gov/air/nitrogenoxides/actions.html#jan10.

[7] Garin, F. Mechanism of NOx decomposition. Appl Catal A: Gen 2001; 222:183–219.

[8] Li Dong. Shiqiu Gao. Guangwen Xu. NO Reduction over Biomass Char in the Combustion Process. Energy Fuels 2010, 24, 446–450.

[9] C.T. Goralski Jr. W.F. Schneider. Analysis of the thermodynamic feasibility of NOx catalysis to meet next generation vehicle NOx emissions standars. Applied Catalysis B: Environmental 37 (2002) 263–277.

[10] Wang, Jinsheng. Jia, Lufei. Anthony, Edward. Mechanism for N2O Formation fomr NO at Ambient Temperature. AIChE Journal 1 (2003) 49.

[11] M.I. Khoder. Atmospheric conversion of sulfur dioxide to particulate sulfate and nitrogen dioxide to particulate nitrate and gaseous nitric acid in an urban area. Chemosphere 49 (2002) 675–684.

[12] Heck, Ronald M. Catalytic abatement of nitrogen oxides–stationary applications. Catalysis Today 53 (1999) 519–523.

[13] G. Di Carlo, L. F. Liotta, G. Pantaleo, A. M. Venezia, G. Deganello. Alumina and Alumina–Baria Supported Cobalt Catalysts for DeNOx: Influence of the Support and Cobalt Content on the Catalytic Performance. Top Catal (2009) 52:1826–1831.

[14] Sun, Wedong. Xu, Liping. Controllable synthesis, characterization and catalytic properties of WO3/ZrO2 mixed oxides nanoparticles. Journal of Colloid and Interface Science 266 (2003) 99-106.

[15] Eriksson, Sara. Nylen, Ulf. Rojas, Sergio. Boutonnet, Magali. Preparation of catalysts from microemulsions and their applications in heterogeneous catalysis. App Cat A: Gen 265 (2004) 207-219.

[16] M. Pileni. "Reverse micelles as microreactors." J. Phys. Chem. 97 (1993) 6961-6973.

[17] Vijay, Rohit. Discovery and Mechanistic Investigation of NOx traps and NH3 Decomposition catalysts using High-Throughput Experimentation. PhD Thesis. University of Delaware. 2007.
[18] Zhang, Xin. Chan, Kwong-Yu. Microemulsion synthesis and electrocatalytic properties of platinum-cobalt nanoparticles. J. Mater, Chem. (2002), 12, 1203-1206.
[19] Lasko, Steven. Hendershot, Reed. Fu, Yu. Snively, Christopher. Lauterbach, Jochen. Spectroscopic Imaging in the Mid-Infrared Applied to High-Throughput Studies of Supported Catalyst Libraries. High-Throughput Analysis by Potyrailo and Amis (2003).
[20] Roberts. M.W. The Formation of N2) during the chemisorptions of nitric oxide at platinum surfaces at low temperatures: a comment on the mechanism. Cat. Letters 93 (2004) 1-2.